A PRELIMINARY STUDY OF A SURFACE WAVE-ACOUSTICAL NORMAL MODE RESONANCE IN A FLUID-FILLED RECTANGULAR WAVEGUIDE WITH PRESSURE-RELEASE BOUNDARIES

Norman Ewing Davis

NAVAL POSTGRADUATE SCHOOL
Monterey, California

THESIS

A PRELIMINARY STUDY
OF A SURFACE WAVE-ACOUSTICAL NORMAL MODE
RESONANCE IN A FLUID-FILLED RECTANGULAR
WAVEGUIDE WITH PRESSURE-RELEASE BOUNDARIES

by

Norman Ewing Davis

and

Morton William Kenyon

December 1974

Thesis Advisor: A.B. Coppens

Approved for public release; distribution unlimited.

REPORT DOCUMENTATION PAGE

READ INSTRUCTIONS BEFORE COMPLETING FORM

1. REPORT NUMBER
2. GOVT ACCESSION NO.
3. RECIPIENT'S CATALOG NUMBER

4. TITLE (and Subtitle)
A Preliminary Study of a Surface Wave-Acoustical Normal Mode Resonance in a Fluid-Filled Rectangular Waveguide with Pressure-Release Boundaries

5. TYPE OF REPORT & PERIOD COVERED
Master's Thesis; December 1974

6. PERFORMING ORG. REPORT NUMBER

7. AUTHOR(s)
Norman Ewing Davis
Morton William Kenyon

8. CONTRACT OR GRANT NUMBER(s)

9. PERFORMING ORGANIZATION NAME AND ADDRESS
Naval Postgraduate School
Monterey, California 93940

10. PROGRAM ELEMENT, PROJECT, TASK AREA & WORK UNIT NUMBERS

11. CONTROLLING OFFICE NAME AND ADDRESS
Naval Postgraduate School
Monterey, California 93940

12. REPORT DATE
December 1974

13. NUMBER OF PAGES
69

14. MONITORING AGENCY NAME & ADDRESS (if different from Controlling Office)
Naval Postgraduate School
Monterey, California 93940

15. SECURITY CLASS. (of this report)
Unclassified

15a. DECLASSIFICATION/DOWNGRADING SCHEDULE

16. DISTRIBUTION STATEMENT (of this Report)

Approved for public release; distribution unlimited.

17. DISTRIBUTION STATEMENT (of the abstract entered in Block 20, if different from Report)

18. SUPPLEMENTARY NOTES

19. KEY WORDS (Continue on reverse side if necessary and identify by block number)
Normal Mode, Waveguide, Perturbation Resonance, Wave Propagation, Wave Interaction, Sinusoidal Waves, Sinusoidal Surfaces, Ducted Propagation, Perturbation Solution

20. ABSTRACT (Continue on reverse side if necessary and identify by block number)

Studies of the effects of sinusoidal surface waves on the propagation of sound in a waveguide reveal a significant resonance effect under certain "matching" conditions of the wavelength of the surface wave and the wavelength of the acoustical sound field.

An acoustic waveguide with constant cross-section and pressure release boundaries was designed with a termination to

(20. ABSTRACT Continued)

minimize reflection of both surface and acoustic waves so that traveling surface waves and traveling acoustic waves could be generated simultaneously.

With acoustic and surface waves present, the existence of predicted resonances was verified and a strong resonance was examined for comparison with theory. The predicted effects have been qualitatively and quantitatively supported.

A Preliminary Study of a Surface Wave-Acoustical Normal Mode Resonance in a Fluid-Filled Rectangular Waveguide with Pressure-Release Boundaries

by

Norman Ewing Davis
Lieutenant Commander, United States Navy
B.S.E.E., University of Washington, 1964

and

Morton William Kenyon
Lieutenant Commander, United States Navy
B.E.E., Villanova University, 1965

Submitted in partial fulfillment of the requirements for the degree of

MASTER OF SCIENCE IN ENGINEERING ACOUSTICS

from the

NAVAL POSTGRADUATE SCHOOL
December 1974

ABSTRACT

Studies of the effects of sinusoidal surface waves on the propagation of sound in a waveguide reveal a significant resonance effect under certain "matching" conditions of the wavelength of the surface wave and the wavelength of the acoustical sound field.

An acoustic waveguide with constant cross-section and pressure release boundaries was designed with a termination to minimize reflection of both surface and acoustic waves so that traveling surface waves and traveling acoustic waves could be generated simultaneously.

With acoustic and surface waves present, the existence of predicted resonances was verified and a strong resonance was examined for comparison with theory. The predicted effects have been qualitatively and quantitatively supported.

TABLE OF CONTENTS

LIST OF ILLUSTRATIONS

LIST OF SYMBOLS

x, y, z	rectangular coordinates
ℓ_y, ℓ_z	waveguide dimensions
k	acoustic wave number
λ	acoustic wave length
ω	angular frequency of the acoustic signal
c	free field acoustic phase speed
Φ	acoustic velocity potential
Φ_o	unperturbed acoustic velocity potential
Φ_1	perturbed acoustic velocity potential
ε	perturbation constant
t	time
α	acoustic absorption coefficient due to medium
η	acoustic absorption coefficient in x-direction
β	spatial absorption coefficient in z-direction
δ	surface wave attenuation constant
Ω	angular frequency of surface wave
A	surface wave amplitude
$\varepsilon F(x,t)$	surface fluctuation
γ	surface wave number
g	acceleration due to gravity
T	surface tension
ρ	density
h	channel depth
M	modulation parameter

f_r	acoustic resonant frequency
f_s	surface wave frequency
m/n	perturbation ratio
V	velocity of surface wave

ACKNOWLEDGMENT

The authors wish to acknowledge the support and encouragement provided them by Associate Professor A. B. Coppens. The expertise of model make Robert Moeller proved invaluable in the design and construction of the apparatus. In addition, the authors wish to thank technicians Jack Brennan, Dick Cota and Milton Andrews for their assistance.

I. INTRODUCTION

The propagation of acoustic waves in ducts of non-uniform cross-section has been of interest to theoreticians for the past hundred-odd years. In particular, Lord Rayleigh [1] investigated plane-wave reflection from a sinusoidal surface as early as 1875. J. C. Samuels [2] presented theory describing the propagation of harmonic signals in two-dimensional ducts with slightly rough rigid walls. R. F. Salant [3,4] analytically investigated acoustic plane-wave propagation parallel to two rigid sinusoidal walls. Relationships between surface wavenumber and acoustic wavenumber were described, and decay of the disturbance as a function of distance from the surface was discussed. A. H. Nayfeh [5] developed a perturbation solution for acoustic wave propagation in a hard-walled two-dimensional duct whose walls had weak sinusoidal undulations. Resonance conditions for certain relationships between wavenumbers of the wall undulation and the acoustic mode were discussed. W. E. Jordan, Jr. [6] compared the frequency spectra of acoustic fluctuation and surface fluctuation created by wind-generated waves.

More recent work by R. H. Ebert [7] examined the influence of standing gravity waves on standing acoustic waves in a water-filled waveguide with pressure release boundaries. It was confirmed that an infinite number of resonances exist when the surface wavelength is one-half the acoustic wavelength

in the x-direction. Differences between experiment and theory were attributed primarily to excessive surface-wave amplitude, non-uniform standing-wave patterns, and the assumption that acoustic and surface waves were undamped.

The present work simplifies the experimental problem by examining the case of a traveling acoustic wave perturbed by a traveling surface wave in a waveguide of uniform cross-section with pressure-release boundaries. The investigation includes verification of theoretical resonances in higher modes and study of a strong resonance for qualitative analysis.

II. THEORY

A. THE NON-ABSORPTIVE CASE - RESONANCE CONDITION [1-8]

A rectangular waveguide with cross-sectional dimensions ℓ_z and ℓ_y is excited by a sound source at $x = 0$. The waveguide is acoustically terminated at large x so that there is no reflection of the incident acoustic energy back toward $x = 0$. All other boundaries are pressure release.

A well-known solution of the wave equation for the velocity potential with these boundaries is

$$\Phi = \sin(k_z z)\sin(k_y y)\cos(\omega t - k_x x). \tag{2.1}$$

The k's must satisfy

$$k_z = n\pi/\ell_z \text{ and } k_y = p\pi/\ell_y \tag{2.2}$$

where $n,p = 1,2,3, \ldots$

Let the upper boundary be perturbed by a traveling surface wave of amplitude A. If a perturbation constant is defined as $\varepsilon = A/\ell_z$ the boundary conditions are

$$\Phi = 0 \quad \text{at} \quad \begin{cases} z = 0 \\ z = \ell_z + \varepsilon F(x,t) \end{cases} \tag{2.3}$$

where

$$F(x,t) = -\ell_z \cos(\Omega t - \gamma x). \tag{2.3}$$

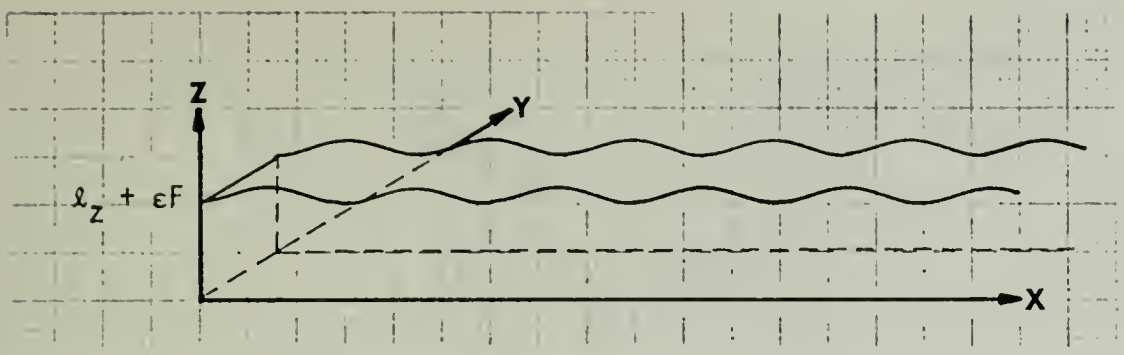

FIGURE 1. THE PERTURBED WAVEGUIDE

Assume there exists a solution

$$\Phi = \Phi_o + \sum_{n=1}^{\infty} \varepsilon^n \Phi_n \tag{2.4}$$

where Φ_o, given by Eq. 2.1, is the solution with an unperturbed boundary, $z = \ell_z$. The boundary conditions are

$$\Phi = 0 \quad \text{at} \quad \begin{cases} z = 0 \\ z = \ell_z. \end{cases}$$

Expansion of $\Phi(z)$ about $z = \ell_z$ in a Taylor's expansion and application of the boundary conditions leads to

$$\Phi_1\Big|_{\ell_z} = - \frac{\partial \Phi_o}{\partial z}\Big|_{\ell_z} F(x,t) \tag{2.5}$$

$$\Phi_2\Big|_{\ell_z} = - \frac{\partial \Phi_1}{\partial z}\Big|_{\ell_z} F(x,t) \tag{2.6}$$

$$\Phi_3\Big|_{\ell_z} = -\left.\frac{\partial \Phi_2}{\partial z}\right|_{\ell_z} F(x,t) - \frac{1}{2!}\left.\frac{\partial^2 \Phi_1}{\partial z^2}\right|_{\ell_z} F^2(x,t) - \frac{1}{3!}\left.\frac{\partial^3 \Phi_o}{\partial z^3}\right|_{\ell_z} F^3(x,t). \tag{2.7}$$

It can be seen that all Φ_n have the same y-dependence as Φ_o. The y-dependent component of Φ_o can be written as $Y(k_y y)$ where $Y(k_y y)$ is the solution to the Helmholtz equation

$$\frac{\partial^2}{\partial y^2} Y + k_y{}^2 Y = 0. \tag{2.8}$$

For the non-absorptive case, Φ and its components must satisfy the lossless wave equation:

$$\Box^2 \Phi = 0, \tag{2.9}$$

$$\Box^2 \Phi_n = 0. \tag{2.10}$$

Examination of the first-order approximation gives

$$\Phi_1\Big|_{\ell_z} = (k_z \ell_z) Y_o \frac{1}{2}\{\cos[(\omega+\Omega)t - (k_x+\gamma)x] + \cos[(\omega-\Omega)t - (k_x - \gamma)x]\}. \tag{2.11}$$

For this boundary condition an acceptable solution is

$$\Phi_1 = \frac{1}{2}(k_z \ell_z) Y \{ \frac{\sin K_z^+ z}{\sin K_z^+ \ell_z} \cos[(\omega+\Omega)t - (k_x+\gamma)x] + \frac{\sin K_z^- z}{\sin K_z^- \ell_z} \cos[(\omega-\Omega)t - (k_x-\gamma)x] \} \tag{2.12}$$

where the propagation constant in the z-direction is

$$K_z^{\pm} \doteq k_z [1 - \frac{1 \pm 2(k_x/\gamma)}{(k_z/\gamma)^2}]^{\frac{1}{2}} . \tag{2.13}$$

$K_z^{\pm}$ can be real or imaginary depending on the relative values of k_x/γ and $(k_z/\gamma)^2$. There is a condition of resonance when $K_z^{\pm}$ is real and

$$K_z^{\pm} \ell_z = m\pi \qquad \text{where } m = 1,2,3 \ldots . \tag{2.14}$$

Note that K_z^+ is imaginary in most of the region where $k_x/\gamma > 0$ and therefore there is no resonance due to K_z^+. K_z^- will be referred to hereafter simply as K_z.

Equation 2.2 stated

$$k_z = \frac{n\pi}{\ell_z} \qquad \text{where } n = 1,2,3 \ldots .$$

therefore a resonance will occur where

$$(\frac{m}{n})^2 \doteq 1 - \frac{1 - 2(k_x/\gamma)}{(k_z/\gamma)^2} . \tag{2.15}$$

The relationship between k_x/γ and $(k_z/\gamma)^2$ for the resonance condition can now be written

$$\frac{k_x}{\gamma} = -\frac{1}{2}[(k_z/\gamma)^2 - 1] + \frac{1}{2}(\frac{m}{n})^2(\frac{k_z}{\gamma})^2 \quad . \tag{2.16}$$

Since resonances occur only when K_z is real,

$$\frac{1 - (2k_x/\gamma)}{(k_z/\gamma)^2} \leq 1 \quad . \tag{2.17}$$

As can be seen in Figure 2 the theoretical plot of k_x/γ vs $(k_z/\gamma)^2$ is a linear relationship for the various perturbation modes.

B. THE ABSORPTIVE CASE - PROPERTIES NEAR RESONANCE [8]

The wave equations for the acoustic potentials in the absorptive case can be written as

$$(\Box^2 - 2\frac{\alpha_o}{c_o}\frac{\partial}{\partial t})\ \Phi_o = 0 \tag{2.18}$$

$$(\Box^2 - 2\frac{\alpha_n}{c_o}\frac{\partial}{\partial t})\ \Phi_n = 0 \tag{2.19}$$

where α_o and α_n are the coefficients of absorption due to all acoustical losses, and can be considered approximately equal in magnitude if Φ_o and Φ_n have similar form.

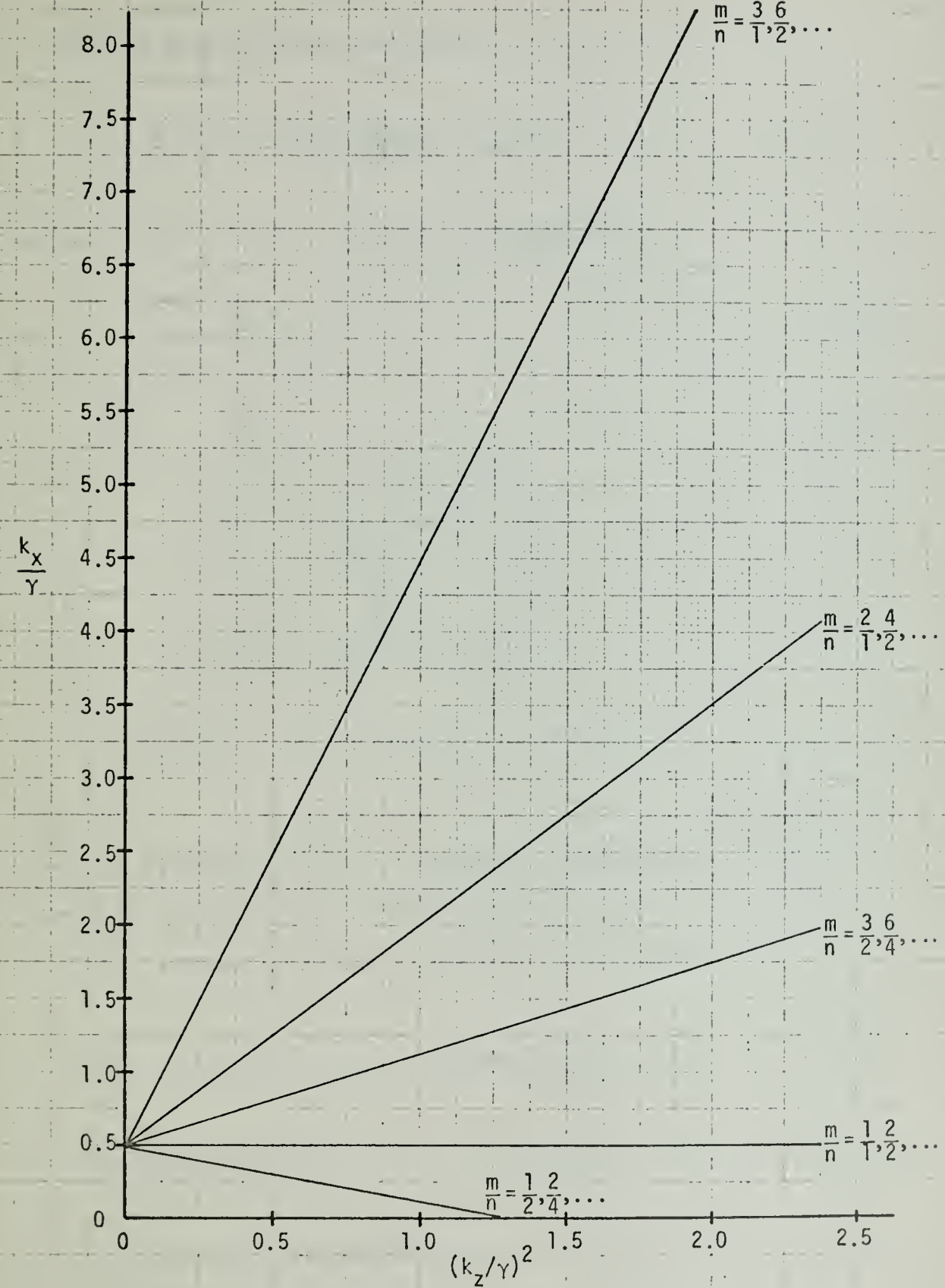

FIGURE 2. THEORETICAL RESONANCE CURVES

Let Φ and Φ_n be of the form

$$Y(k_y y)Z(k_z z)\exp[i(\omega t - \underline{k}_x x)]$$

where $\underline{k}_x = k_x - i\eta_n$. It can be shown that

$$\eta_n = \frac{\omega}{k_x}\frac{\alpha_n}{c_o} \tag{2.20}$$

$$= \frac{\alpha_n}{\cos\ \sigma} \tag{2.21}$$

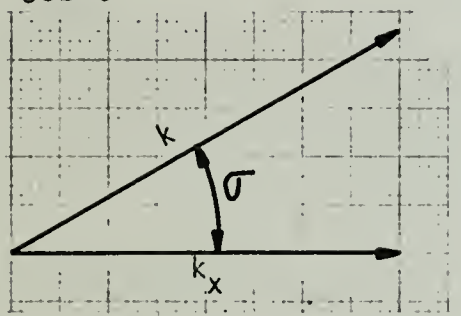

FIGURE 3. RELATIONSHIP OF k AND k_x

where η is the acoustic absorption coefficient in the x-direction and can be determined empirically.

The classical solution, Eq. 2.1, now becomes

$$\Phi_o = \exp(-\eta_o x)Y_o(k_y y)\sin k_z z\exp[i(\omega t - k_x x)] \ . \tag{2.22}$$

If there is surface wave attenuation, Eq. 2.3 is rewritten

$$F(x,t) = -\ell_z\exp(-\delta x)\cos(\Omega t - \gamma x) \tag{2.23}$$

where the surface wave attenuation constant δ can also be determined empirically.

To determine the damping in the z-direction, assume Φ has the form

$$\Phi = Y(k_y y)\exp(-i\underline{K}_z z)\exp[i(\omega-\Omega)t]\exp[-i(k_x-\gamma)x] \exp[-(\eta+\delta)x] \tag{2.24}$$

where $\underline{K}_z = K_z - i\beta$.

Substitution of this equation into Eq. 2.19 shows that the spatial decay in the z-direction, β, is given by

$$\beta = \frac{\alpha_1 k - (\eta+\delta)(k_x - \gamma)}{K_z} . \tag{2.25}$$

The perturbed solution, Eq. 2.12 then becomes

$$\Phi_1 = \frac{1}{2}(k_z \ell_z) Y \frac{\sin \underline{K}_z z}{\sin \underline{K}_z \ell_z} \exp[-(\eta+\delta)x]\exp\{i[(\omega-\Omega)t-(k_x-\gamma)x]\} \tag{2.26}$$

where

$$\Delta K_z = K_z - k_z \quad \text{and} \quad \Delta\varphi \equiv \tan^{-1} \frac{\beta \ell_z}{\Delta K_z \ell_z} . \tag{2.27}$$

The first order solution for the acoustic potential, $\Phi = \Phi_o + \Phi_1$, in the vicinity of a resonance near an antinode in the transverse directions (y and z) can now be written as

$$\Phi = Y\exp(-\eta x)\exp[i(\omega t - k_x x)]\{\sin k_z z + \frac{\varepsilon\pi}{2} R\exp(i\Delta\varphi)\exp[i(\Omega t - \gamma x)]\} \tag{2.28}$$

where

$$R = \left| \frac{\sin \pi z/\ell_z}{(\Delta K_z \ell_z)^2 + (\beta \ell_z)^2} \right| \quad z \neq 0, \ell_z \tag{2.29}$$

and

$$\varepsilon = \varepsilon_o \exp(-\delta x) \ . \tag{2.30}$$

The total solution can be viewed as a sum of a fixed and a rotating phasor as shown in Figure 4. The modulation parameter, M, is defined to be

$$M = \tfrac{1}{2}\pi\varepsilon_o R\exp(-\delta x) \ . \tag{2.31}$$

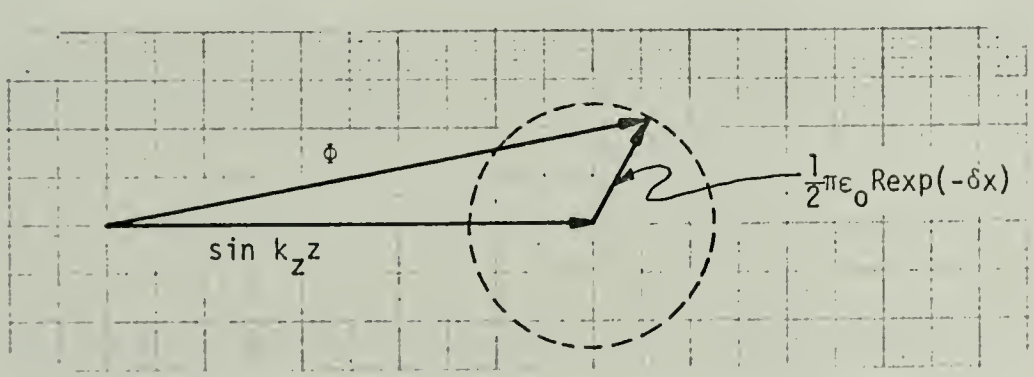

FIGURE 4. PHASOR REPRESENTATION OF SOLUTION

C. COMPUTATION OF ACOUSTIC FREQUENCY AND SURFACE WAVE NUMBER - RESONANCE CONDITION

Substitution of Eq. 2.2 into Eq. 2.16 yields

$$k_x/\gamma = \frac{1}{2}[m^2 - n^2](\frac{\pi}{\ell_z \gamma})^2 + \frac{1}{2} \tag{2.32}$$

which states the relationship between the acoustic wave number in the x-direction and the surface wave number for a given perturbation ratio, m/n. The relationship between k_x and the acoustic angular frequency ω is given by

$$k_x = [(\frac{\omega}{c})^2 - k_z^2 - k_y^2]^{\frac{1}{2}} . \tag{2.33}$$

When $\ell_z = \ell_y$, application of Eq. 2.2 gives

$$k_x = [(\frac{\omega}{c})^2 - (n^2 + p^2)(\frac{\pi}{\ell_z})^2]^{\frac{1}{2}} \tag{2.34}$$

which can be written as

$$\frac{\omega}{c} = [k_x^2 + (n^2 + p^2)(\frac{\pi}{\ell_z})^2]^{\frac{1}{2}} . \tag{2.35}$$

The angular cutoff frequency of this square waveguide is

$$\frac{\omega_{np}}{c} = [(n^2 + p^2)(\frac{\pi}{\ell_z})^2]^{\frac{1}{2}} . \tag{2.36}$$

Squaring Eq. 2.36 and substitution into Eq. 2.36 yields

$$\frac{\omega}{c} = \left[k_x^2 + \left(\frac{\omega_{np}}{c}\right)^2\right]^{\frac{1}{2}} \tag{2.37}$$

which can be written as

$$\omega = \left[k_x^2 c^2 + \omega_c^2\right]^{\frac{1}{2}}. \tag{2.38}$$

In terms of the acoustic frequency, Eq. 2.38 becomes

$$f = \left[\left(\frac{k_x}{2\pi}\right)^2 c^2 + \left(\frac{\omega_c}{2\pi}\right)^2\right]^{\frac{1}{2}} \tag{2.39}$$

$$= \left[\left(\frac{c}{\lambda_x}\right)^2 + f_c^2\right]^{\frac{1}{2}} . \tag{2.40}$$

Thus for a given γ, the two values of k_x given by Eq. 2.32 could result in the same acoustic frequency for different combinations of normal mode, (n,p) and perturbation ratio, m/n. The acoustic frequency and surface wave number may be degenerate at one point only or they may be coincident throughout the range of resonant acoustic frequency and surface wave number. In this latter case the different combinations of the normal mode and perturbation ratio are termed degenerate modes. For example, a comparison of Figure 14, for the (1,1) normal mode with perturbation ratio m/n = 2/1 with Figure 16 for the (2,1) normal mode with perturbation ratio m/n = $\frac{1}{2}$, reveals degenerate modes.

III. EXPERIMENT

A. DESCRIPTION OF THE SYSTEM

An acoustic waveguide with pressure-release boundaries was designed for the experiment (see Figures 5, 6, and 7). The size was chosen to provide a uniform water column 10 centimeters square and 1.52 meters in length. These dimensions produced a calculated cut-off frequency for the lowest mode of 10.466 kHz, for a speed of sound in water of $c = 1480$ m/sec. The walls, constructed of one-inch thick polyurethane foam, thinly coated with liquid neoprene to provide strength and minimize wetting of the foam, closely approximated pressure release surfaces as verified by pressure probe measurements.

A waveguide termination, designed to minimize reflections of the acoustic wave, consisted of a 20 inch section of an exponential horn and a 16 inch V-shaped closure. The horn was constructed of styrofoam and the closure was lined with sound-absorbent aluminum-impregnated rubber. An angle of 60° in the closure assured that a plane wave propagating in a straight path down the waveguide would suffer at least two reflections before being reflected back into the channel.

To reduce surface wave reflections, a "beach" was constructed, consisting of a wire screen tray cut to fit the 60° closure, and penetrating the surface of the water to a depth of about one centimeter. The tray was filled with stainless steel ribbon shavings to dissipate the surface wave energy.

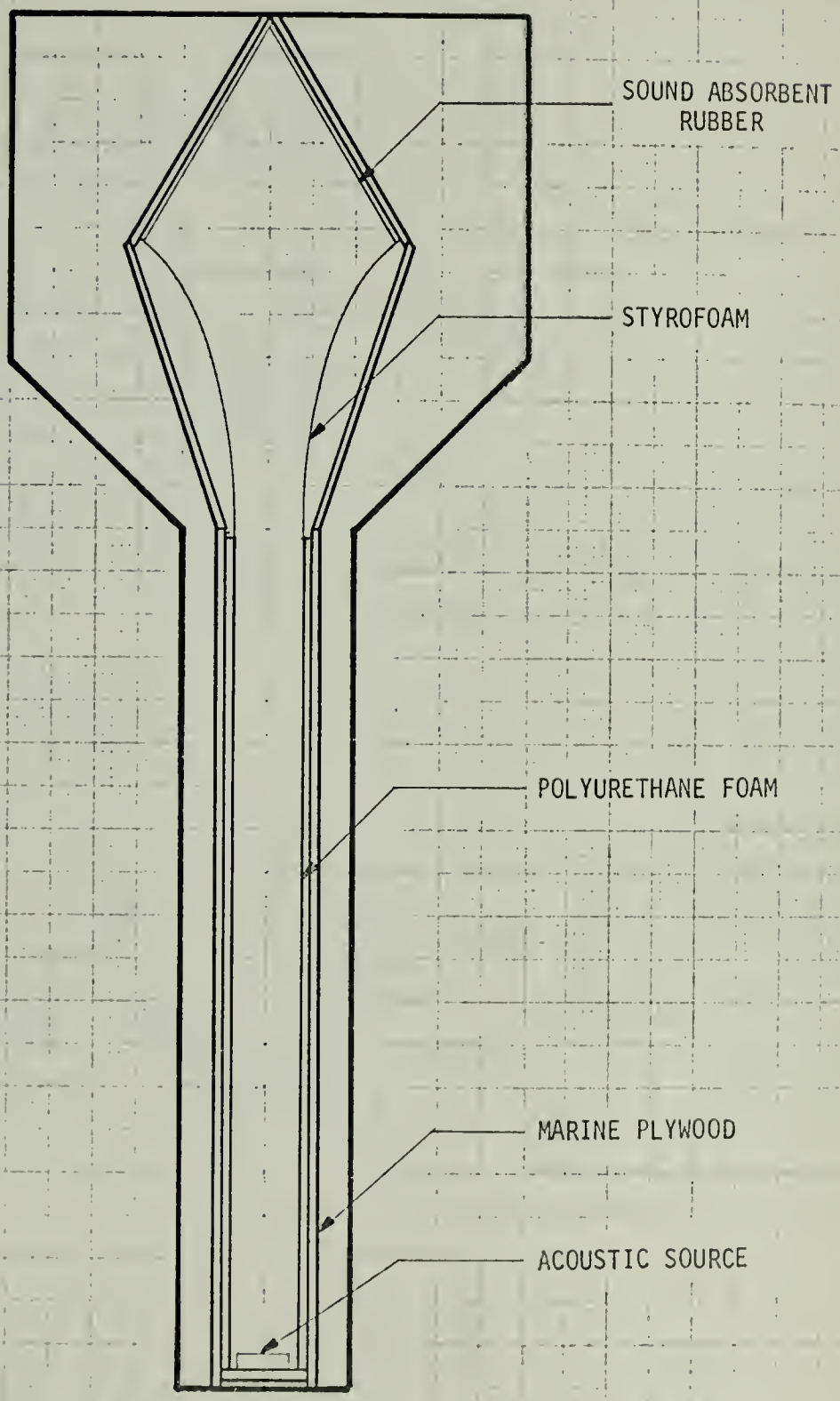

FIGURE 5. PLAN VIEW OF ACOUSTIC WAVEGUIDE

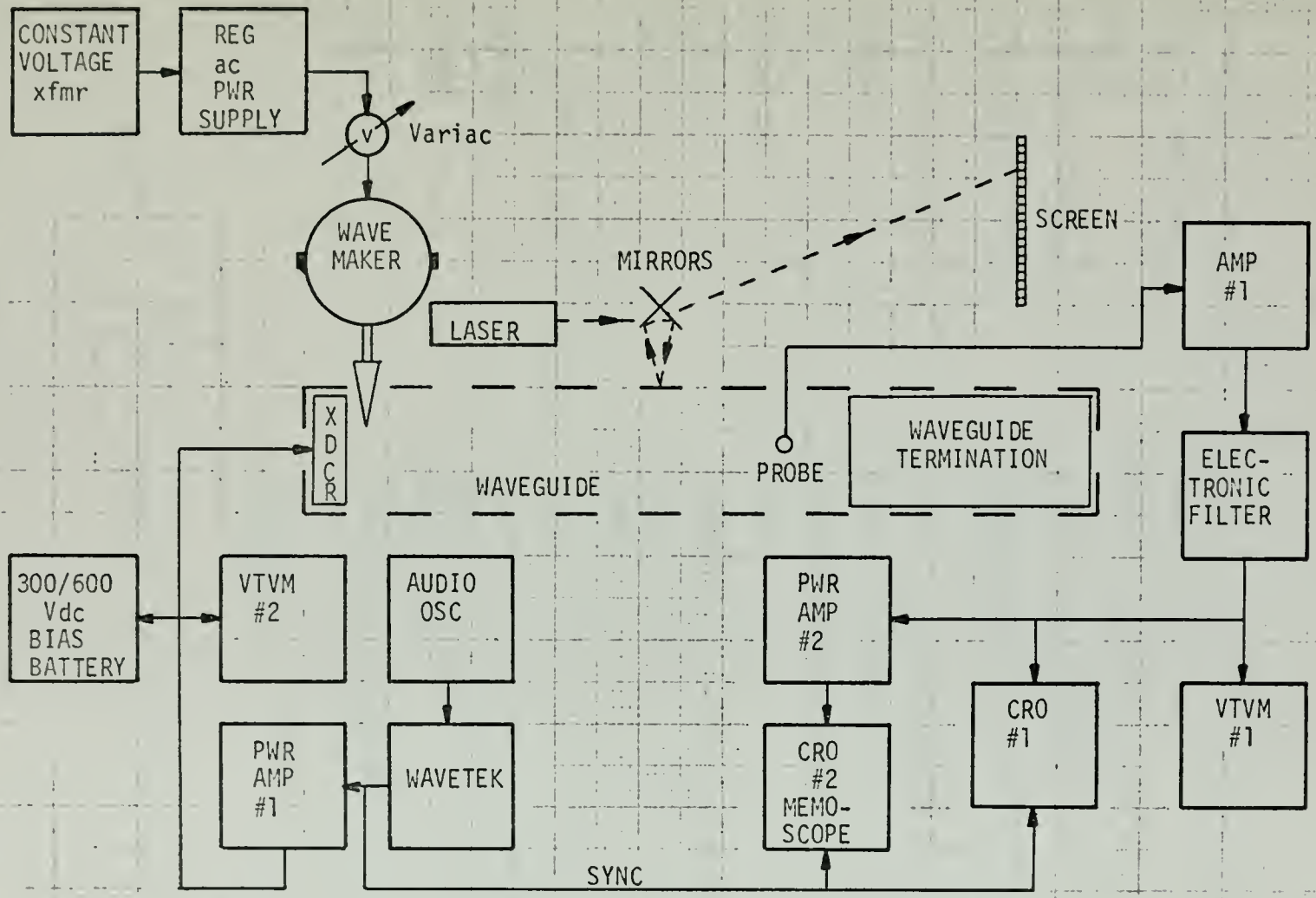

FIGURE 6. BLOCK DIAGRAM OF SYSTEM

Constant Voltage xfmr	SOLA Electric Company #30974
Reg ac Pwr Supply	CENCO # 79642
Amp #1	Hewlett Packard Model 465A
Pwr Amp #1 and #2	Hewlett Packard Model 467A
Electronic Filter	Spencer-Kennedy Laboratories, Inc., Model 302
VTVM #1 and #2	Hewlett Packard Model 400D
CRO #1	Hewlett Packard Model 120B
CRO #2	Hughes MEMOSCOPE Model 105
Audio Osc	CENCO #80593
WAVETEK	WAVETEK Multi-purpose VCG Model 116
Laser	C. W. Radiation, Inc., 0.5 mW HeNe Laser
300/600 Vdc Bias Battery	Burgess U200 300V "B" Battery
Variac	Superior Electric Co. POWERSTAT
Probe	CELESCO Industries Hydrophone Model LC5-2
Xdcr	Locally Manufactured MYLAR Electrostatic Source
Wave Maker	Locally Manufactured Surface Agitator

FIGURE 7. LIST OF EQUIPMENT SHOWN IN FIGURE 6

The surface waves were generated by means of a variable-speed ac motor rotating an adjustable cam attached to a driving arm. The driving arm was connected to a wedge of plexiglas which penetrated the surface of the water and generated surface waves by vertical oscillatory motion. The surface wave frequency could be adjusted in the range 2-6 Hz by varying the supply voltage to the motor. The frequency was measured by means of a cam-driven microswitch which actuated an electromechanical counter. Wave amplitude could be adjusted in the range 0-5 mm by varying the eccentricity of the cam and was determined by a slope-detecting optical system described in Figure 8. A laser was used to provide an intense, collimated beam of light which was reflected onto the perturbed surface of the water by a set of mirrors which could be traversed in the x-direction. The reflected light was projected to a screen over a long path length. The system was calibrated by mounting a small mirror on a one meter bar and then reflecting the light beam from this mirror instead of the water surface. The bar was then set at known angles while the deflection of the beam on the screen was measured. The observed deflection was proportional to the angle of inclination of the bar over the range of interest.

The acoustic field was generated by a plane MYLAR electrostatic source polarized with a 300V battery. The active face of the source was 3 in. square. The signal

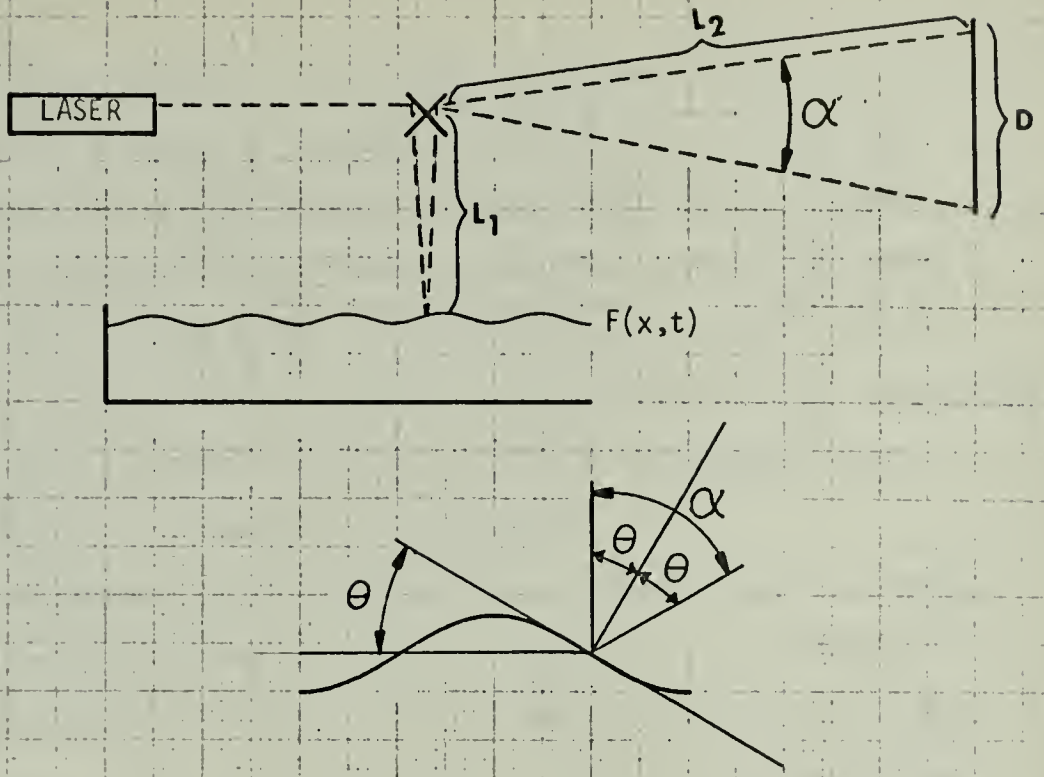

$F(x,t) = A\cos(\Omega t - \gamma x)$ $\qquad \frac{dF}{dx} = -A\gamma\sin(\Omega t - \gamma x) \doteq \theta$

$\theta_{max} = A\gamma$ $\qquad L = L_1 + L_2$

$\alpha = \tan^{-1}(D/L)$ $\qquad D = \alpha L$

$\alpha = 2\theta_{max}$ $\qquad D = 2A\gamma L$

$$A = D/(2\gamma L)$$

FIGURE 8. THE SLOPE-DETECTION OPTICAL SYSTEM

voltage was provided by a signal generator which could be operated in either CW or pulsed modes. The CW mode was used when taking data and the pulsed mode was used when "tuning" the system for minimum acoustic reflection from the far end of the guide. The system was "tuned" by adjusting the number and position of triangular sound-absorbent rubber wedges within the throat of the exponential horn until minimum reflection was observed.

The acoustic probe (CELESCO Model LC5-2) was a ceramic hydrophone with a useful frequency range of 1 - 600 kHz, and a nominal sensitivity of -126 dB RE 1V/microbar within this range. The signal from the hydrophone was amplified by 40 dB to provide proper oscilloscope presentation. A bandpass filter was used to reject signals below 9 kHz and above 40 kHz. Figures 9, 10 and 11 show the system.

B. DESCRIPTION OF THE EXPERIMENTS

The object was to study the fluctuations in the acoustic pressure amplitude of a traveling wave resulting from the interaction of the acoustic field with a sinusoidal surface wave in the case where both surface and acoustic waves were traveling waves. In particular, the existence of predicted resonances was to be verified, and a single resonance was to be examined quantitatively for comparison with theory.

The first experiment was the investigation of the resonance conditions. The relationship between the velocity V of the

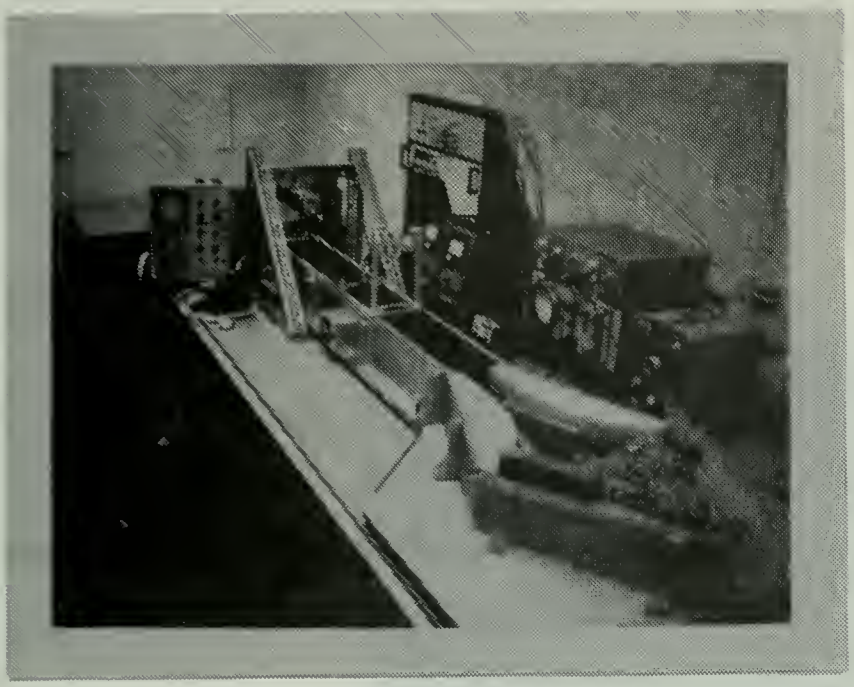

FIGURE 9
THE SYSTEM

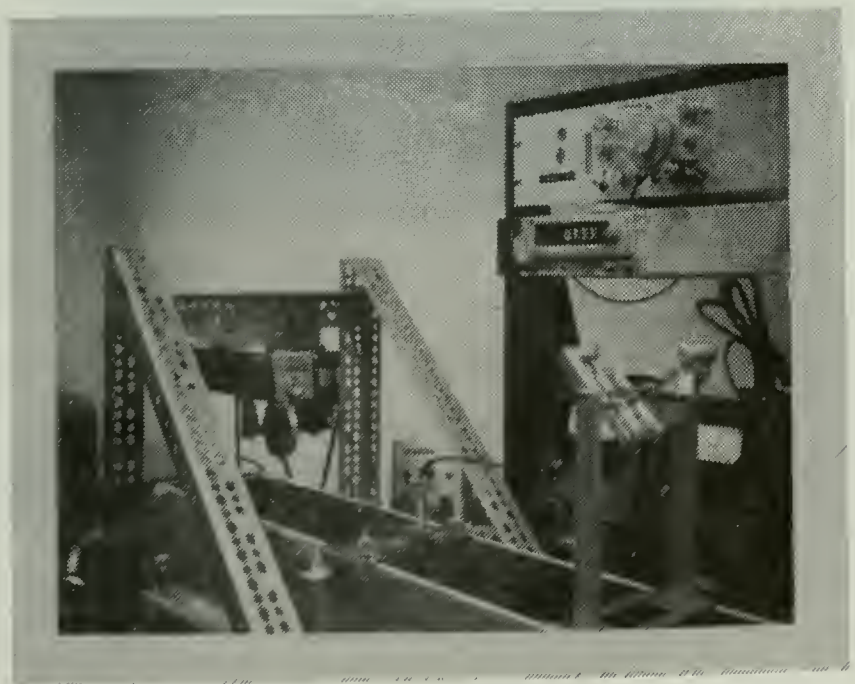

FIGURE 10
DRIVER, PROBE
AND OPTICAL
SYSTEM

FIGURE 11. WAVEGUIDE, BEACH AND OPTICAL SCREEN

surface wave and the surface wave number γ [9] is given by

$$V^2 = (g/\gamma + \frac{T\gamma}{\rho}) \tanh \gamma h \qquad (3.1)$$

Since $V = \Omega/\gamma$,

$$\Omega = \gamma[g/\gamma + T\gamma/\rho]^{\frac{1}{2}} [\tanh \gamma h]^{\frac{1}{2}} . \qquad (3.2)$$

Using Eq. 3.2, γ vs $f_s = \Omega/2\pi$ was computed and is plotted in Figure 12. Equations 2.32 and 2.40 were then utilized in that order to compute the required resonant acoustic frequency for the combination of normal mode and perturbation resonance being investigated. A plot of k_x vs f_r for the various modes is shown in Figure 13. These computations were expedited with the help of a Hewlett Packard Model HP9100A programmable desk calculator.

Starting with the (1,1) normal mode and a given γ, the values of the surface frequency and acoustic frequency were computed for the lowest perturbation resonance, m/n = 1/1. The surface wave generator was set to the selected frequency by counting and averaging the number of cycles over a two minute period. The WAVETEK was then tuned through the general vicinity of the predicted acoustical frequency until a resonant condition was observed. The empirical values of (k_x/γ) and $(k_z/\gamma)^2$ were then computed and plotted.

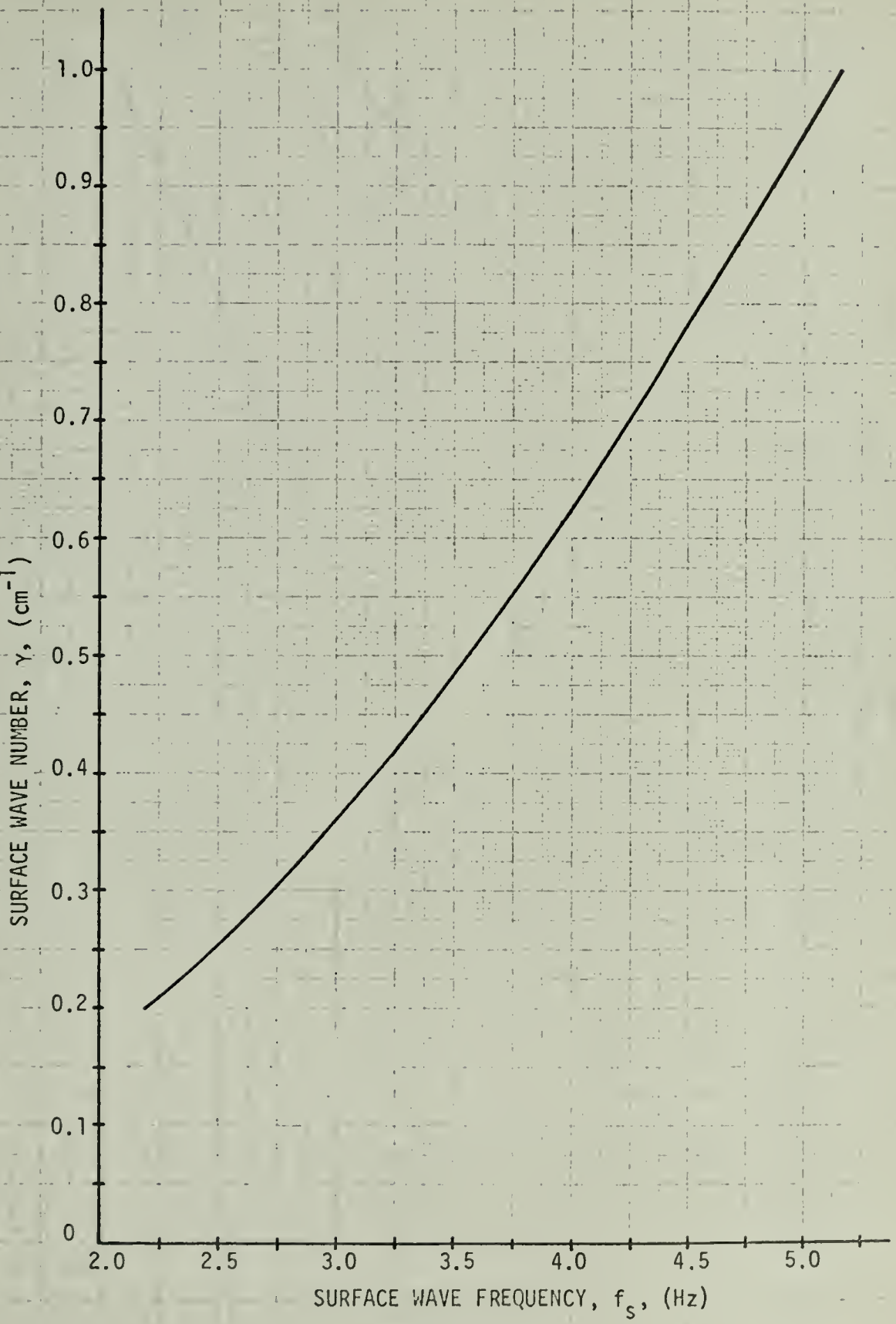
1.0
0.9
0.8
0.7
0.6
0.5
0.4
0.3
0.2
0.1
0
SURFACE WAVE NUMBER, γ, (cm⁻¹)
2.0
2.5
3.0
3.5
4.0
4.5
5.0
SURFACE WAVE FREQUENCY, f_s, (Hz)

FIGURE 12

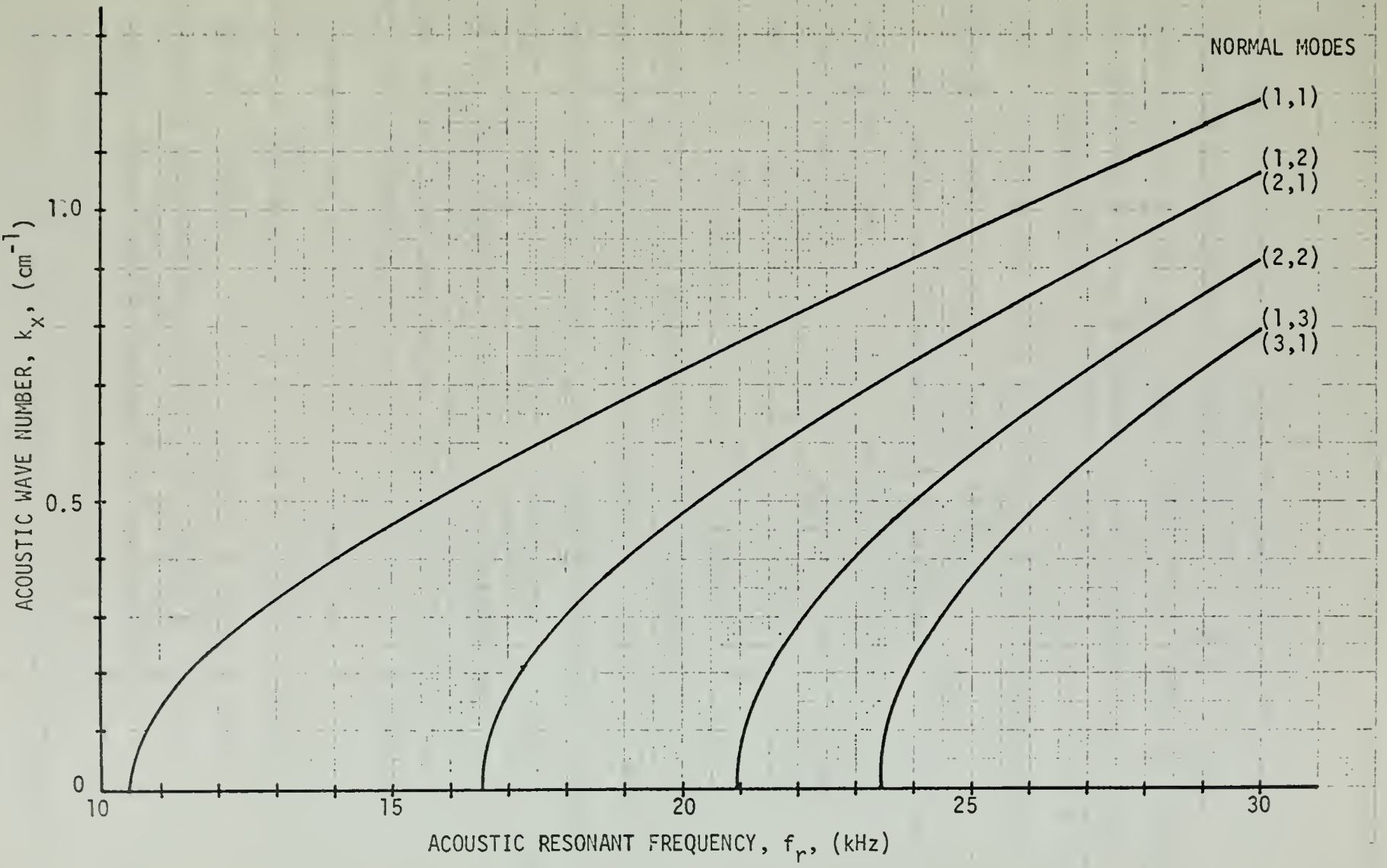
NORMAL MODES
(1,1)
(1,2)
(2,1)
(2,2)
(1,3)
(3,1)
ACOUSTIC WAVE NUMBER, k_x, (cm^{-1})
1.0
0.5
0
10
15
20
25
30
ACOUSTIC RESONANT FREQUENCY, f_r, (kHz)

FIGURE 13

Using the predicted values of acoustic frequencies for the higher perturbation resonances, e.g., m/n = 2/1 and m/n = 3/1, for the (1,1) normal mode, the process was repeated for the same surface frequency. Five surface wave frequencies corresponding to $(k_z/\gamma)^2$ = 1/8, 1/4, 1/2, 1, and 2 were used. These values were selected to give a representative spread on the (k_x/γ) vs $(k_z/\gamma)^2$ curves.

The values of the acoustical frequencies for the (1,1) normal mode, m/n = 2/1 perturbation resonance were above the cut-off frequency for the (1,2) and (2.1) normal modes. Those for the (1,1) normal mode, m/n = 3/1 perturbation resonance, were above the cut-off frequency for the (2,2) normal mode. When operating at an acoustic frequency which was high enough to permit propagation of higher normal modes, interference from these higher modes was observed. Examination of Figs. 14 - 19 and Eq. 2.16 reveals co-incident plots of resonant acoustic frequency f_r vs surface wavenumber for several combinations of normal mode and perturbation resonance. For example, normal mode (1,1), perturbation resonance 2/1 is degenerate with normal mode (2,1), perturbation resonance 1/2. The remainder of these combinations are listed in Table 1. It was necessary to device means to suppress interference between the degenerate modes. The acoustic probe was positioned to take advantage of the symmetry in modal patterns as shown in Figure 20. When the (1,1) normal mode was being investigated, the probe was placed on

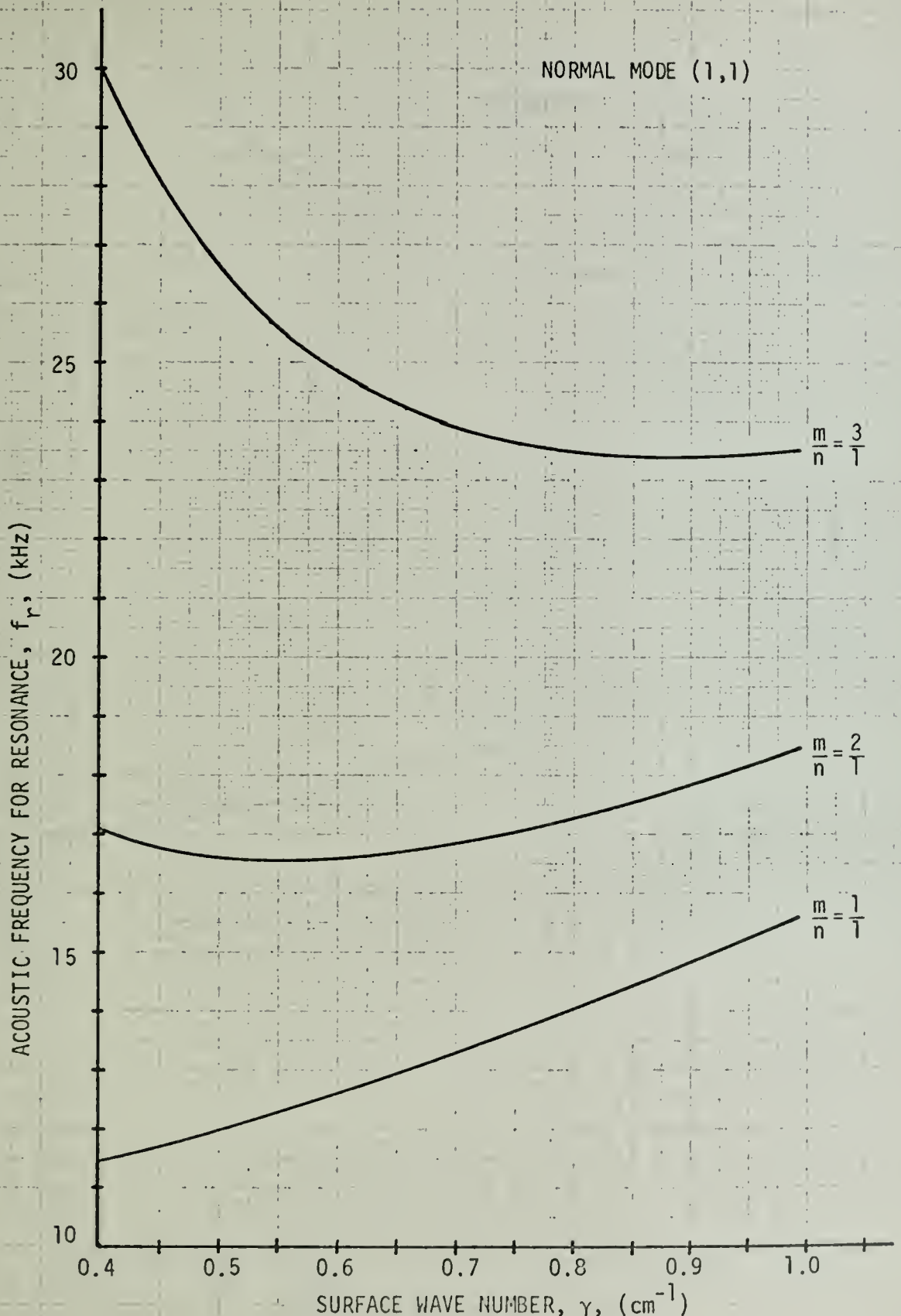
NORMAL MODE (1,1)
30
25
20
15
10
ACOUSTIC FREQUENCY FOR RESONANCE, f_r, (kHz)
$\frac{m}{n} = \frac{3}{1}$
$\frac{m}{n} = \frac{2}{1}$
$\frac{m}{n} = \frac{1}{1}$
0.4
0.5
0.6
0.7
0.8
0.9
1.0
SURFACE WAVE NUMBER, γ, (cm^{-1})

FIGURE 14

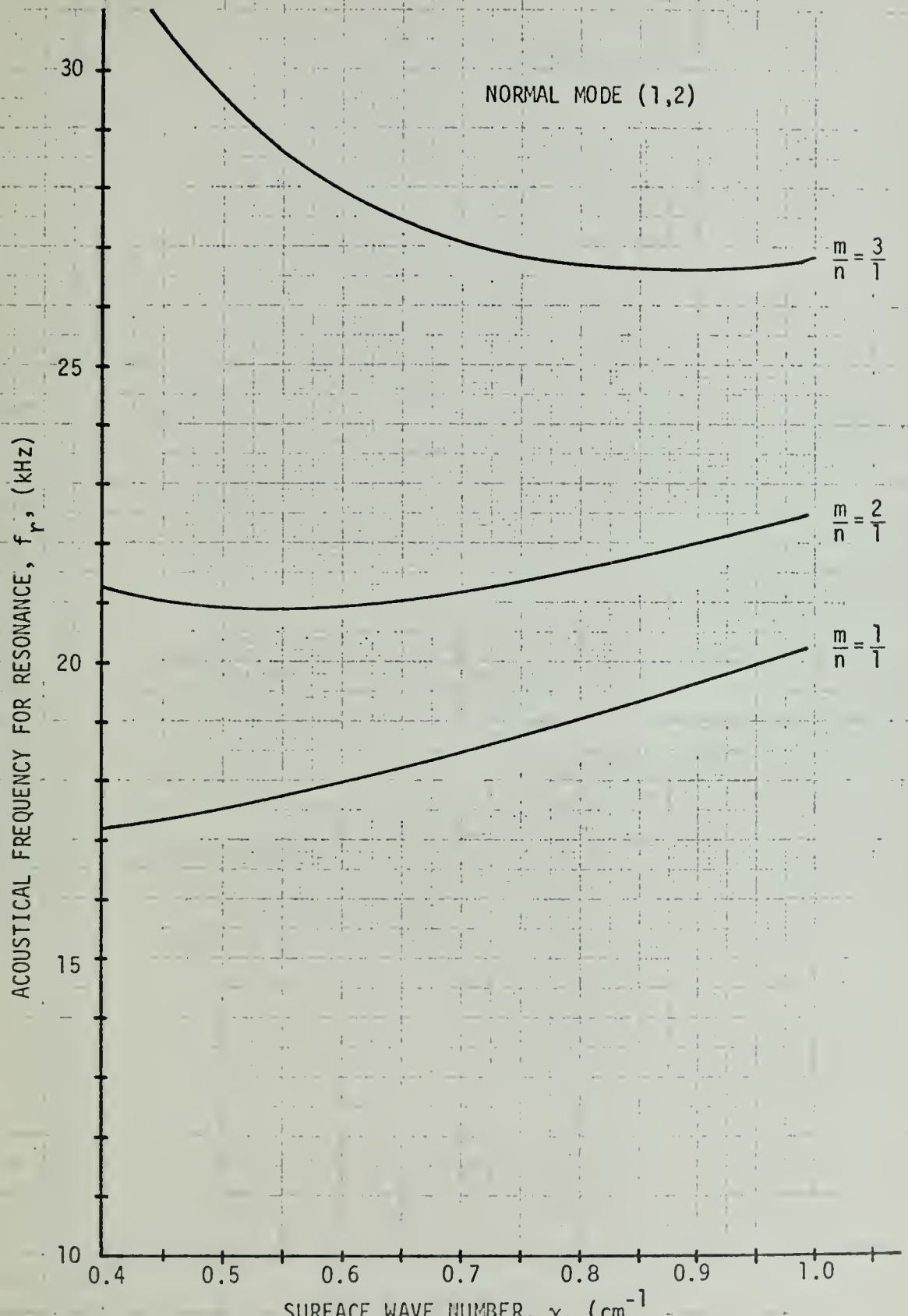
NORMAL MODE (1,2)
m/n = 3/1
m/n = 2/1
m/n = 1/1
ACOUSTICAL FREQUENCY FOR RESONANCE, f_r, (kHz)
30
25
20
15
10
0.4
0.5
0.6
0.7
0.8
0.9
1.0
SURFACE WAVE NUMBER, γ, (cm^{-1})

FIGURE 15

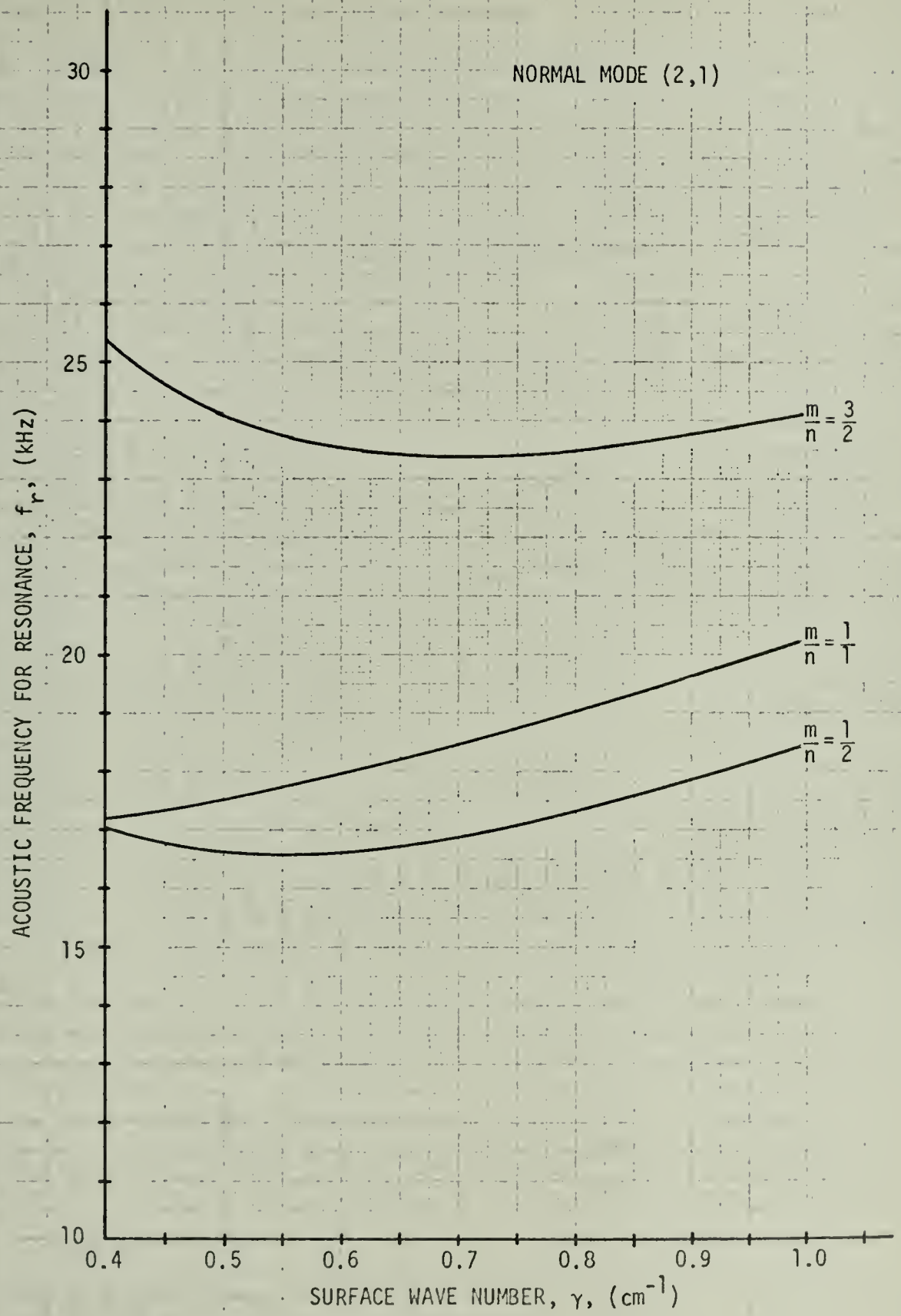
NORMAL MODE (2,1)
30
25
20
15
10
ACOUSTIC FREQUENCY FOR RESONANCE, f_r, (KHz)
$\frac{m}{n} = \frac{3}{2}$
$\frac{m}{n} = \frac{1}{1}$
$\frac{m}{n} = \frac{1}{2}$
0.4
0.5
0.6
0.7
0.8
0.9
1.0
SURFACE WAVE NUMBER, γ, (cm^{-1})

FIGURE 16

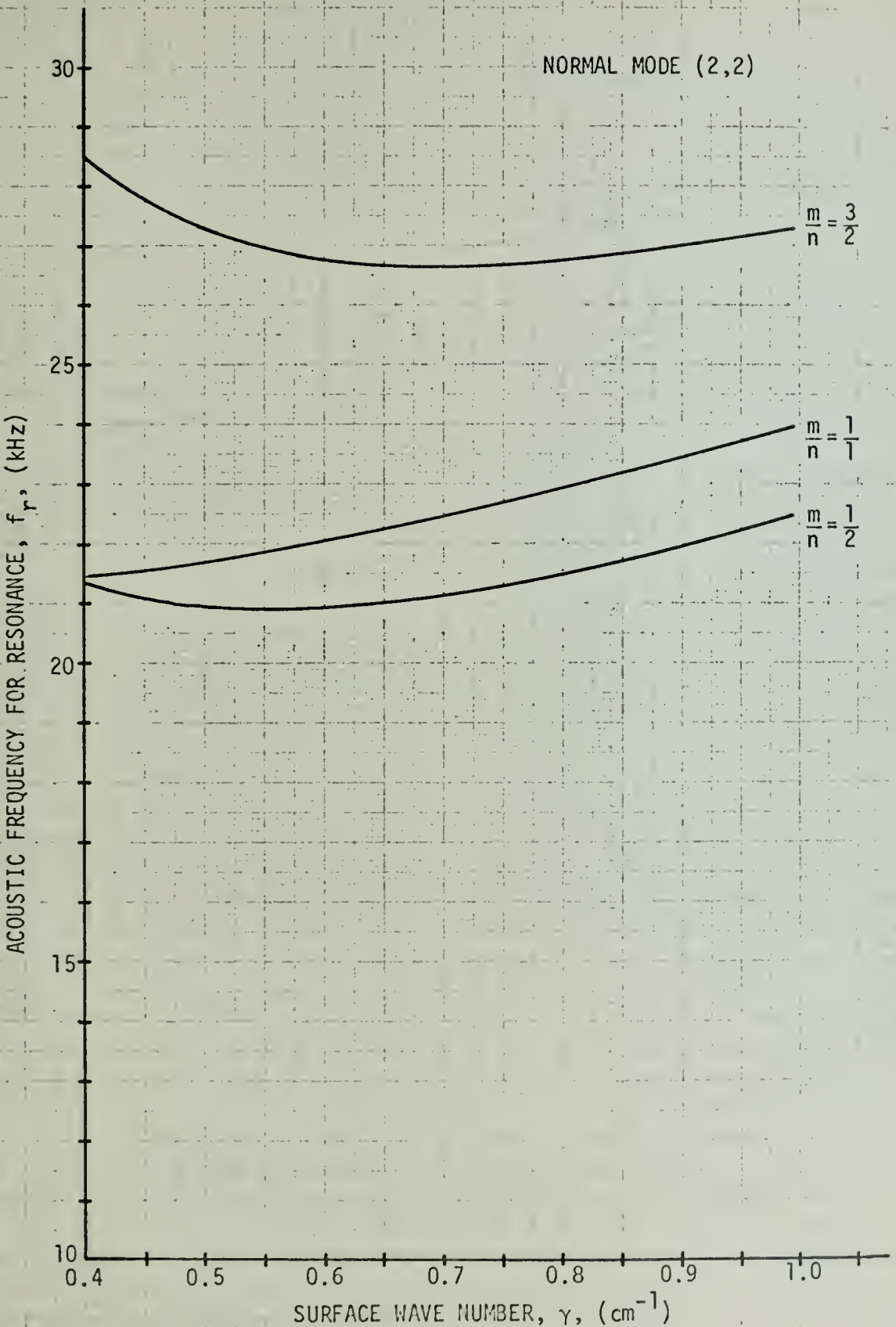
NORMAL MODE (2,2)
30
25
20
15
10
0.4
0.5
0.6
0.7
0.8
0.9
1.0
m/n = 3/2
m/n = 1/1
m/n = 1/2
ACOUSTIC FREQUENCY FOR RESONANCE, f_r, (kHz)
SURFACE WAVE NUMBER, γ, (cm^{-1})

FIGURE 17

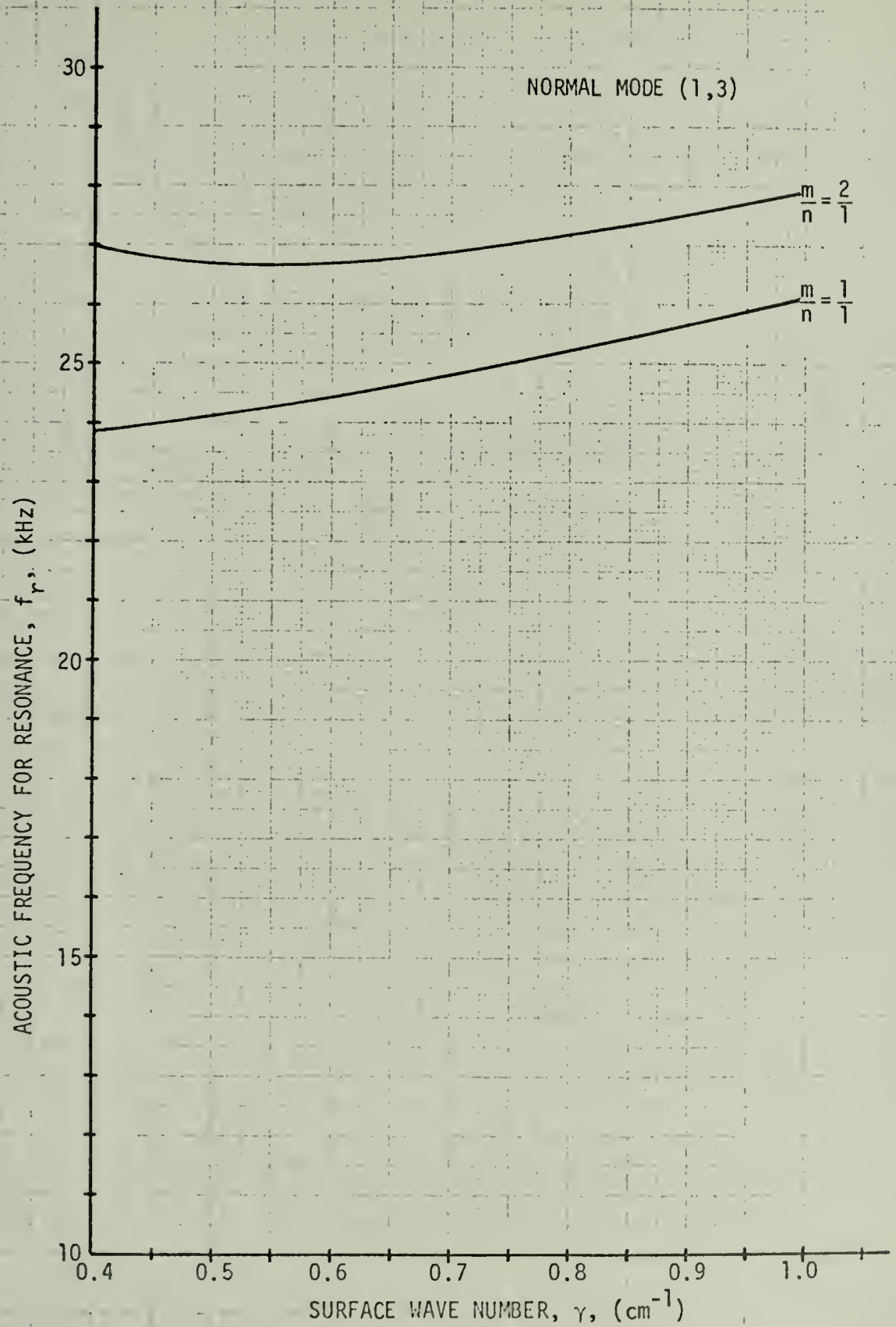
NORMAL MODE (1,3)
m/n = 2/1
m/n = 1/1
30
25
20
15
10
0.4
0.5
0.6
0.7
0.8
0.9
1.0
ACOUSTIC FREQUENCY FOR RESONANCE, f_r, (kHz)
SURFACE WAVE NUMBER, γ, (cm^{-1})

FIGURE 18

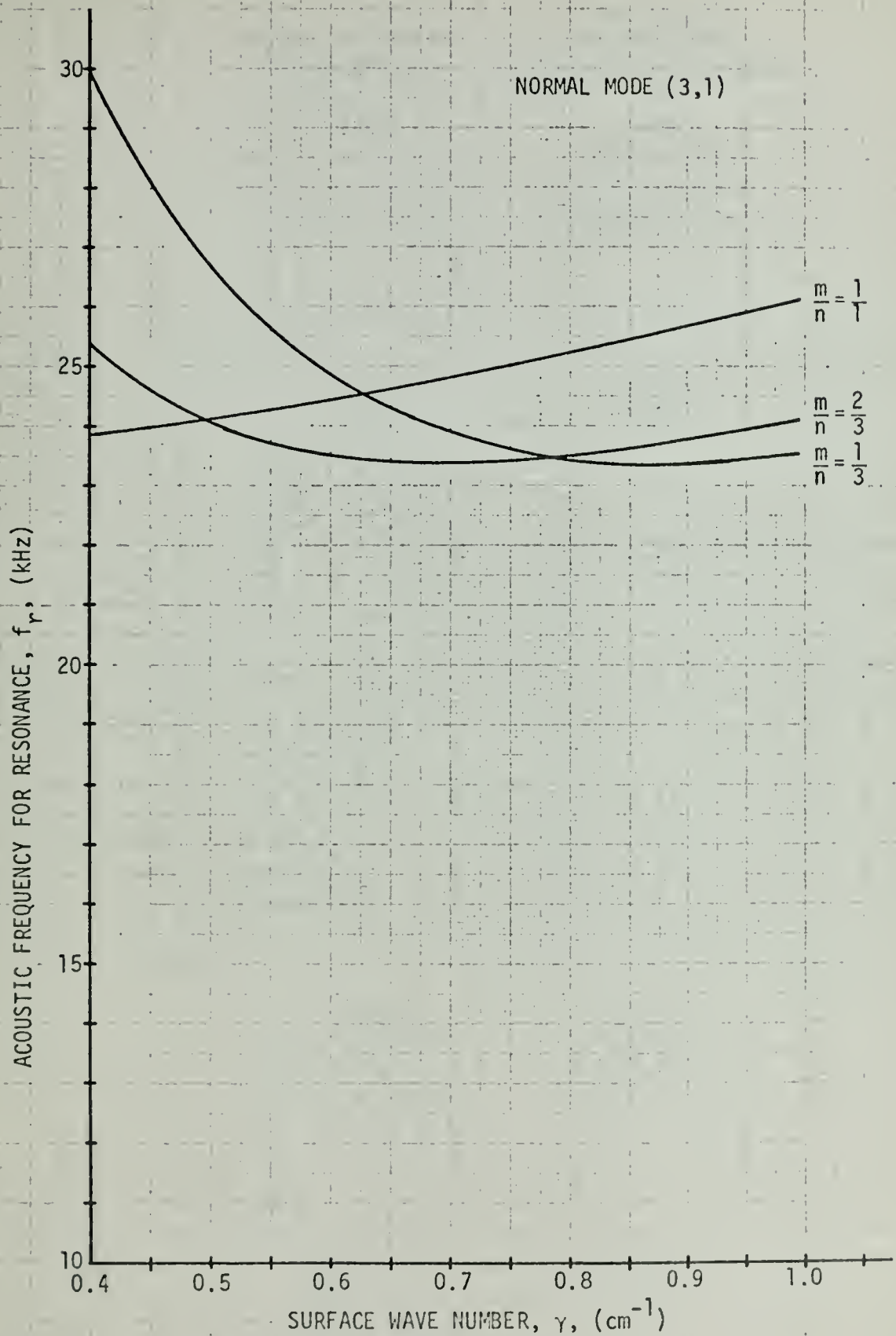
NORMAL MODE (3,1)
m/n = 1/1
m/n = 2/3
m/n = 1/3
ACOUSTIC FREQUENCY FOR RESONANCE, f_r, (kHz)
30
25
20
15
10
0.4
0.5
0.6
0.7
0.8
0.9
1.0
SURFACE WAVE NUMBER, γ, (cm^{-1})

FIGURE 19

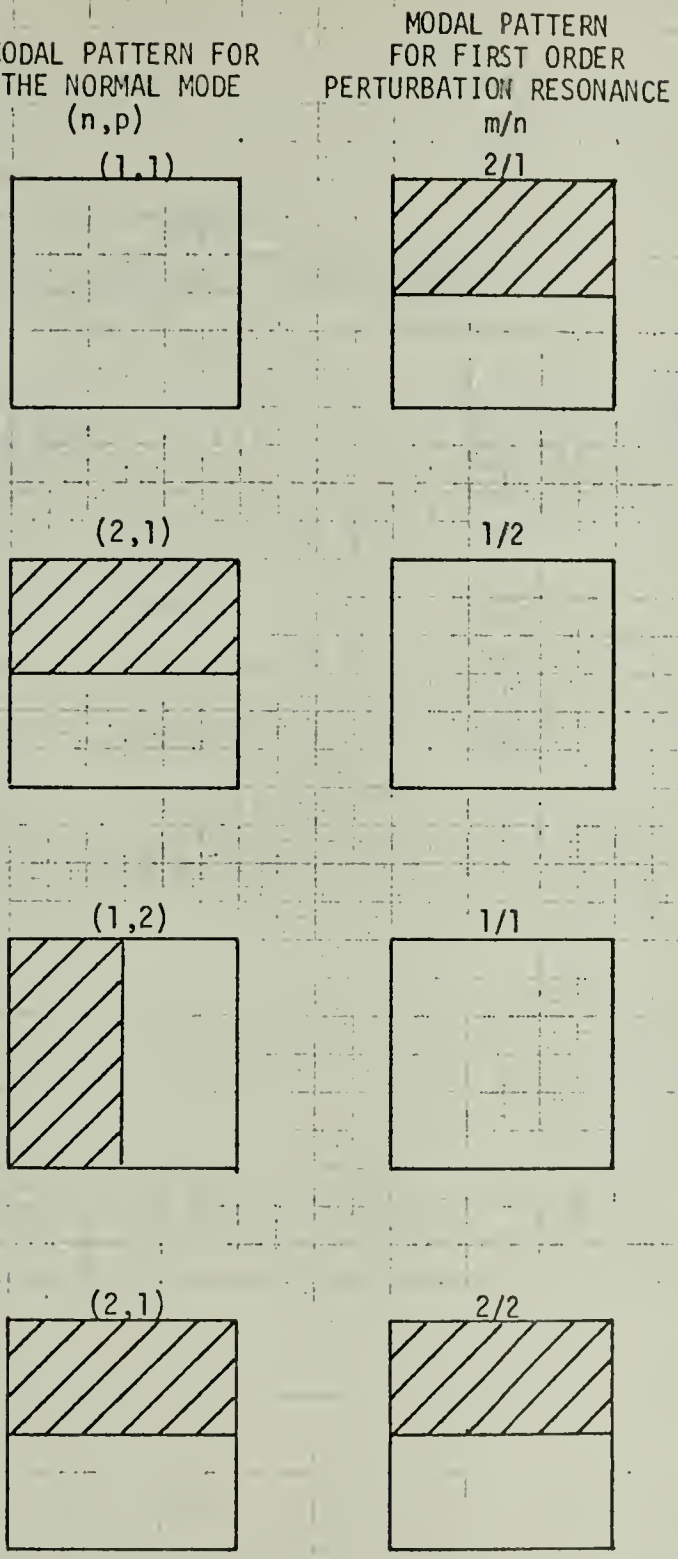

FIGURE 20. MODAL PATTERNS

TABLE 1

DEGENERATE MODE COMBINATIONS

NORMAL MODE	PERTURBATION RESONANCE		NORMAL MODE	PERTURBATION RESONANCE
(1,1)	2/1	degenerate with	(2,1)	1/2
(1,2)	1/1	degenerate with	(2,1)	2/2
(1,2)	2/1	degenerate with	(2,2)	1/2
(1,1)	3/1	degenerate with	(3,1)	1/3
(2,1)	3/2	degenerate with	(3,1)	2/3
(1,3)	1/k	degenerate with	(3,1)	1/1

the center axis of the water column which was a node for the (1,2), (2,1) and (2,2) normal modes. The only degeneracy which could not be suppressed in this manner was the (1,1) normal mode, m/n = 3/1 perturbation resonance which was coincident with the (3,1) normal mode, m/n = 1/3 perturbation resonance as shown in Figure 21. However, it was felt that the symmetry of the source combined with the relative strength of these two modes made the contribution of the (3,1) normal mode insignificant.

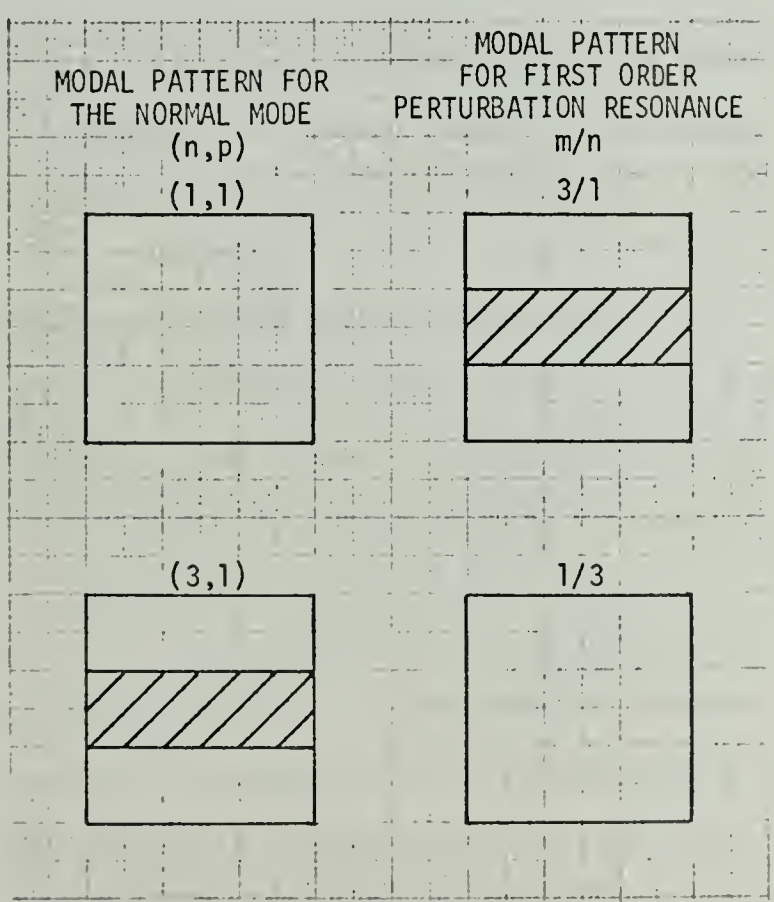

FIGURE 21. UNSUPPRESSED MODAL PATTERNS

To permit investigation of the higher modes, the source was modified to suppress the (1,1) normal mode and enhance the mode in question. A sheet of 1/4 in. neoprene foam was placed over the left half of the source to enhance the (1,2) normal mode, then over the upper half to enhance the (2,1) normal mode. A checkerboard pattern was used to enhance the (2,2) normal mode. Figure 22 shows the data, plotted on the theoretical (k_x/γ) vs $(k_z/\gamma)^2$ curves.

A second portion of the first experiment consisted of searching for unexplained resonances. With the surface frequency fixed, the input signal was tuned from the (1,1) cut-off frequency to the (2,2) cut-off frequency to see if any unexplained resonances could be located. None were found.

The objective of the second experiment was to compare the behavior of the system in the vicinity of a resonance with theoretical predictions. The study was limited to the (1,1) normal mode at the perturbation resonance, m/n = 1/1 to preclude interference from higher normal modes. The surface wave attenuation was determined by measuring the wave height from 40 cm to 120 cm from the driver wedge in 5 cm increments. The slope, δ, of the semi-log plot of the surface wave amplitude vs distance from the source was then computed. This process was repeated at the five surface wave frequencies examined in the first experiment.

At the five corresponding acoustic resonance frequencies, the acoustic pressure probe was traversed over the same range

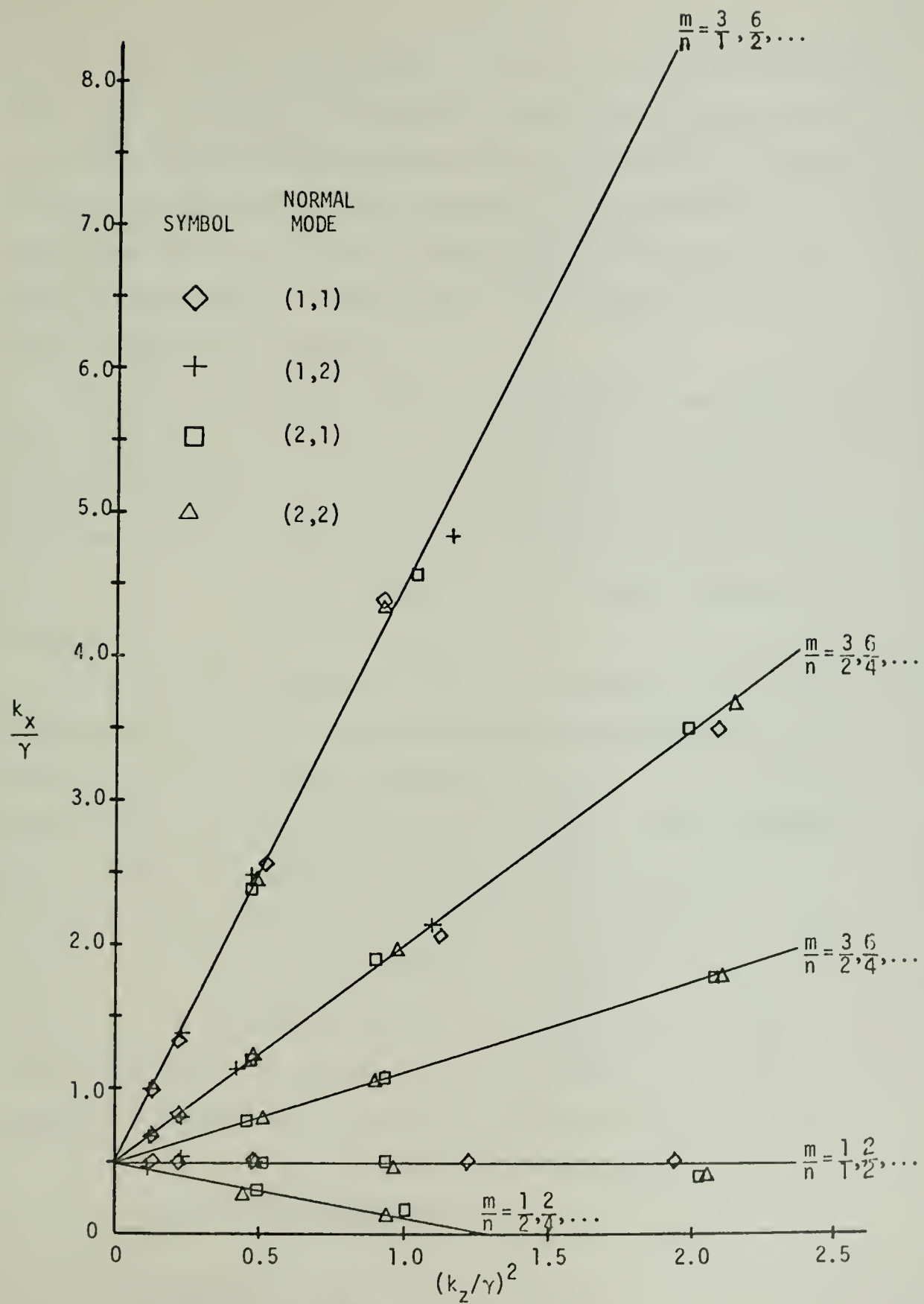

THEORETICAL RESONANCE CURVES WITH DATA

FIGURE 22

as the wave height measurement. The surface was unperturbed. Since there was some reflection of acoustical energy from the termination, readings were taken at nodes and antinodes of the standing wave. The amplitude of the readings at the nodes were plotted on a semi-log plot vs the distance from the transducer. The slopes, η, of these plots were then computed and compared.

One resonance was selected for qualitative and quantitative analysis. The surface wave attenuation constant δ and acoustic absorption coefficient in the x-direction η were measured both before and after data were taken. The absorption coefficient in the z-direction β was then computed using Eq. 2.25.

With the wave generator set at a frequency of 4.2 Hz the acoustic signal was set at various frequencies in the vicinity of the resonant frequency of 13.25 kHz. The frequency band of interest was 12.5 - 14.0 kHz. The MEMOSCOPE was triggered in single sweep mode and amplitude data were read from the CRT display. Figure 23 is a graphical illustration of the display and Figures 24 and 25 show typical examples of strongly and weakly modulated signals. The data taken were the values of 2a + 2b and 2a - 2b. The modulation parameter, M = b/a was then computed as follows

$$X = \left[1 - \frac{2a - 2b}{2a + 2b}\right] \times 100 \qquad (3.3)$$

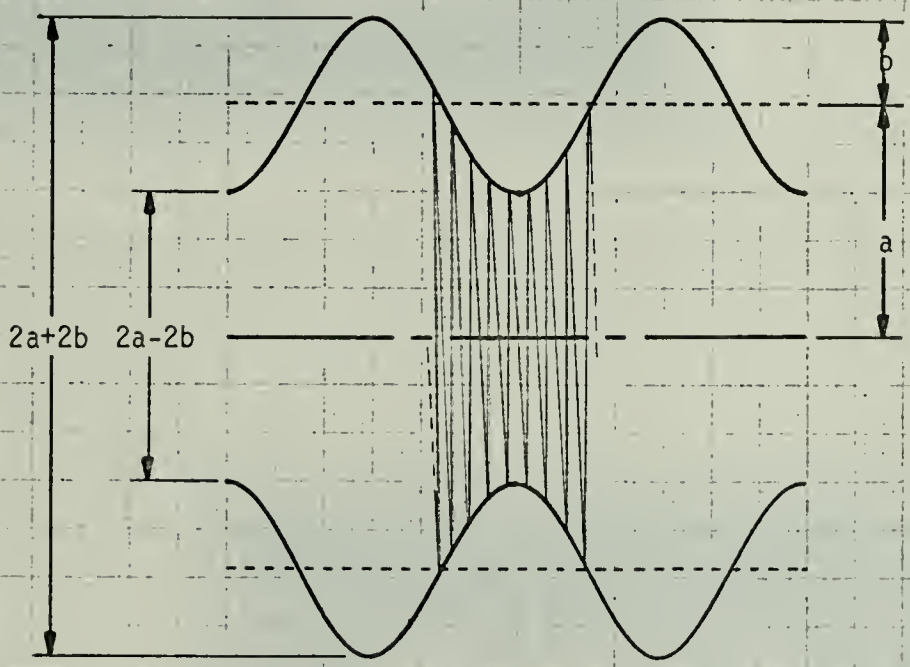

FIGURE 23. MEASUREMENT OF MODULATION PARAMETER

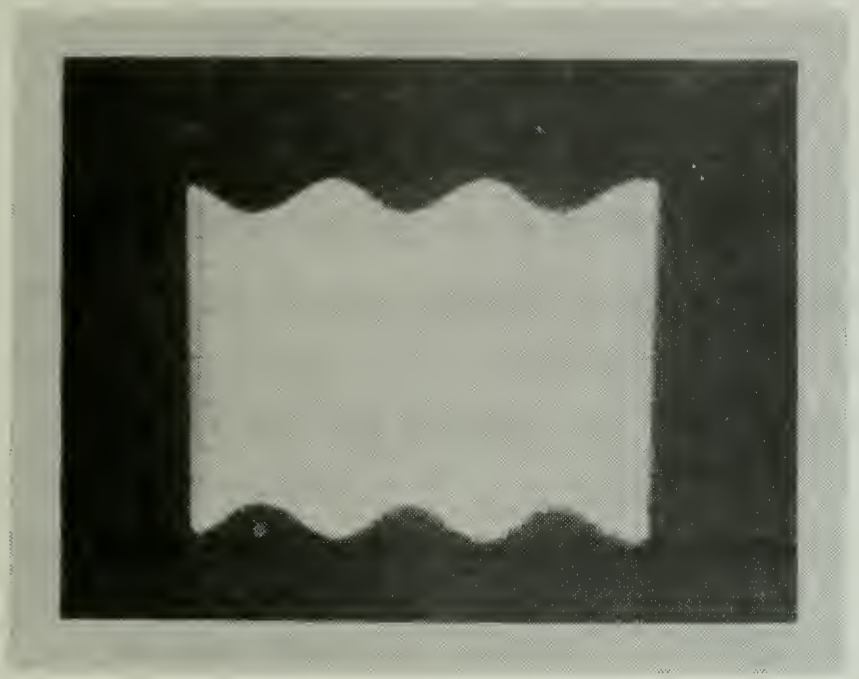

FIGURE 24

STRONG
MODULATION

FIGURE 25

WEAK
MODULATION

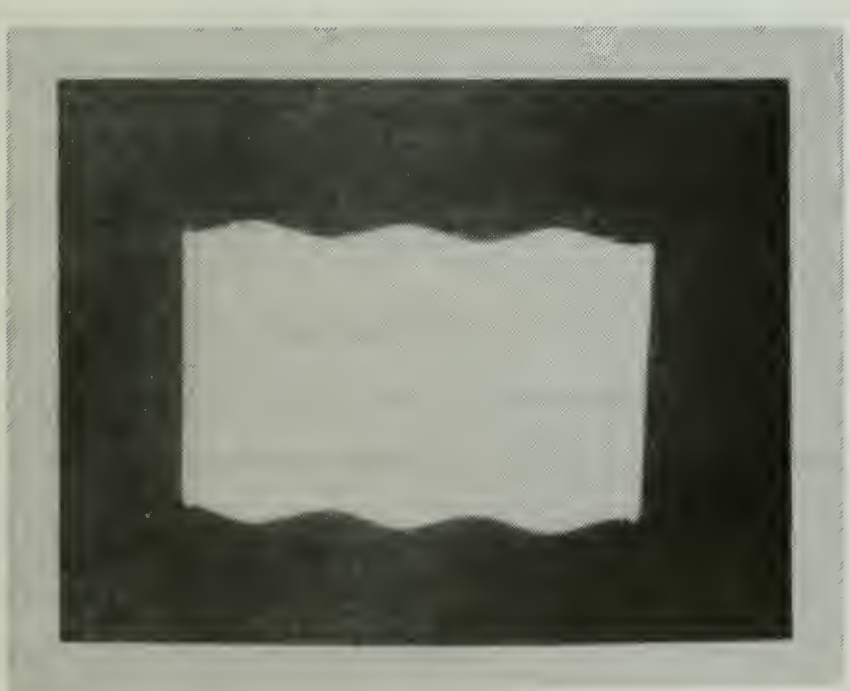

$$M = \frac{b}{a} = \frac{X}{200 - X} \cdot \qquad (3.4)$$

Eight sets of data were taken. The acoustic probe was positioned at each of four distances from the source: 42, 67, 90, and 100 cm. Four runs were completed at the 42 cm position, one at the 67 cm position, two at the 90 cm position, and one at the 100 cm position. The data are shown in Figures 26 - 33.

C. ERROR ANALYSIS

The perturbation constant, ε, which is the ratio of waveheight to water column depth depends upon how precisely the waveheight could be determined. The deflection of the laser beam on the wall screen could be read accurately to ±1 cm and the path length determined to ±3 cm. Assuming that the waveguide was uniform to within ±1 % of the measured dimensions, ε becomes

$$\varepsilon_o = \frac{D \pm 1}{(\ell_z \pm 0.01\ \ell_z)2\gamma(L \pm 3)} \qquad (3.5)$$

where all dimensions are in centimeters.

This yields an uncertainty in the measurement of ε_o of ±5 %. The experimental determination of the surface wave attenuation constant, δ, resulted in a ±5 % error from "worst case" graphical interpretations. The in situ value of ε was dependent upon the relationship

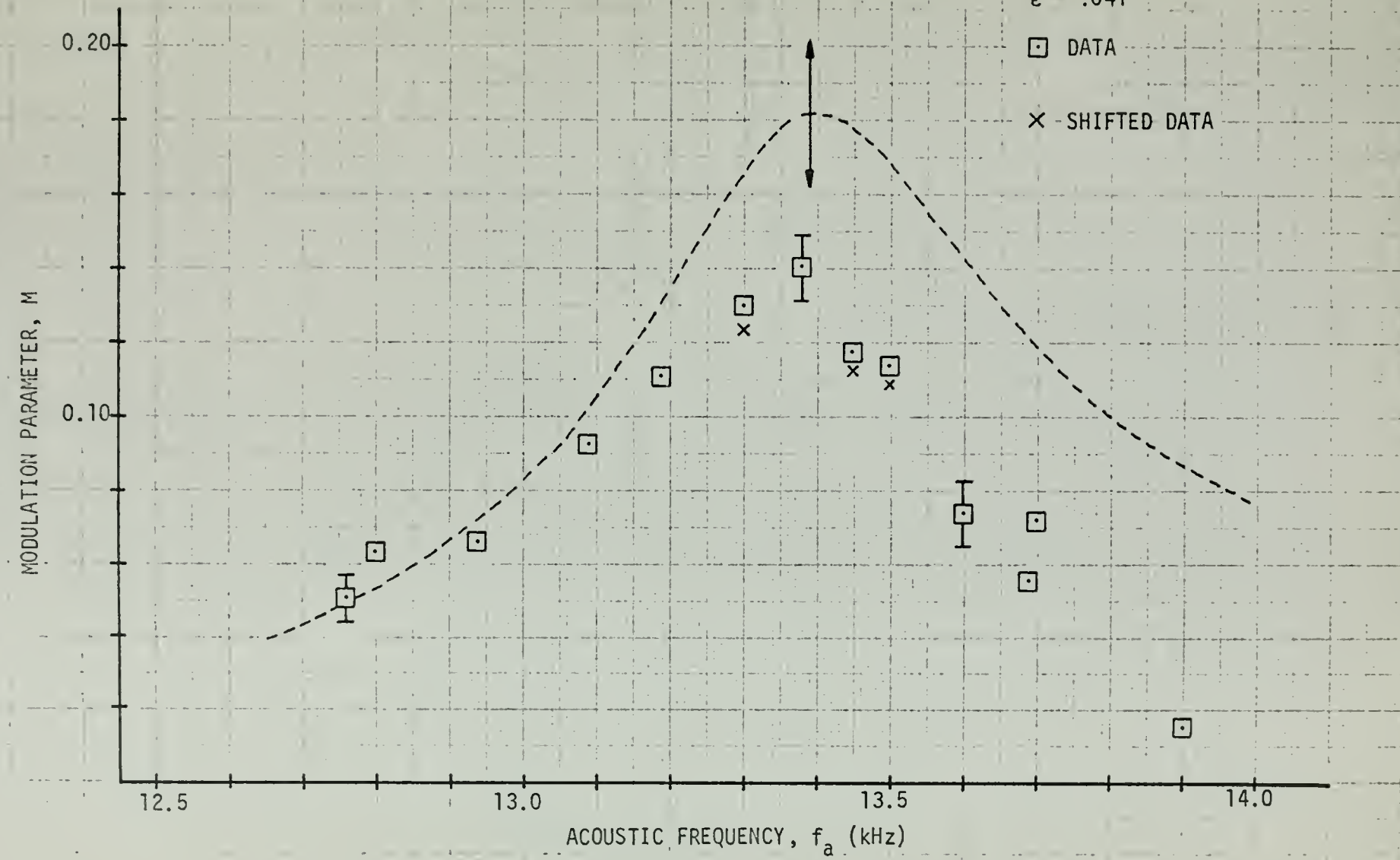
PROBE POSITION 42 cm
ε = .041
DATA
SHIFTED DATA
0.20
0.10
MODULATION PARAMETER, M
12.5
13.0
13.5
14.0
ACOUSTIC FREQUENCY, f_a (kHz)

FIGURE 26

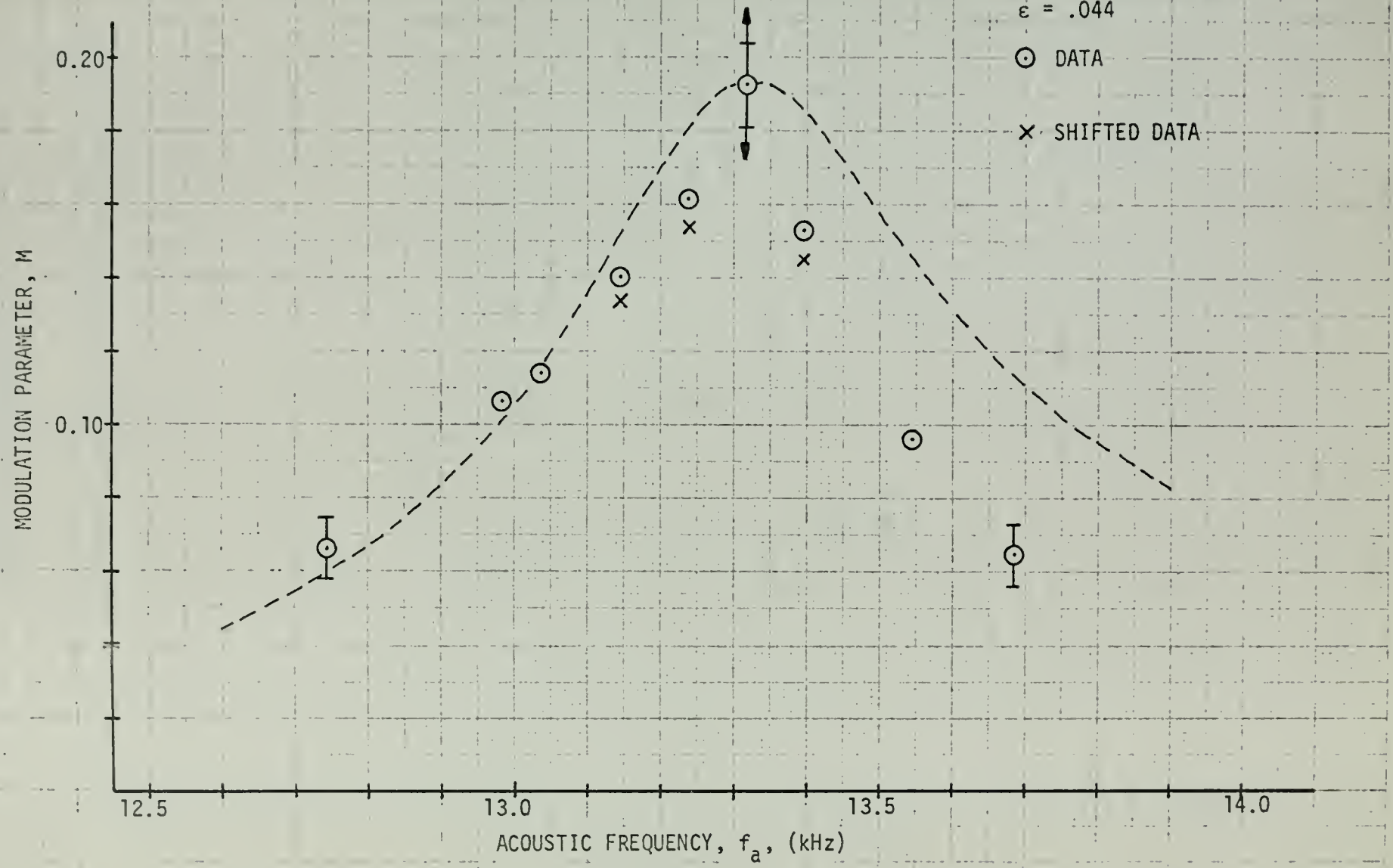
PROBE POSITION 42 cm
ε = .044
DATA
SHIFTED DATA
0.20
0.10
MODULATION PARAMETER, M
12.5
13.0
13.5
14.0
ACOUSTIC FREQUENCY, f_a, (kHz)

FIGURE 27

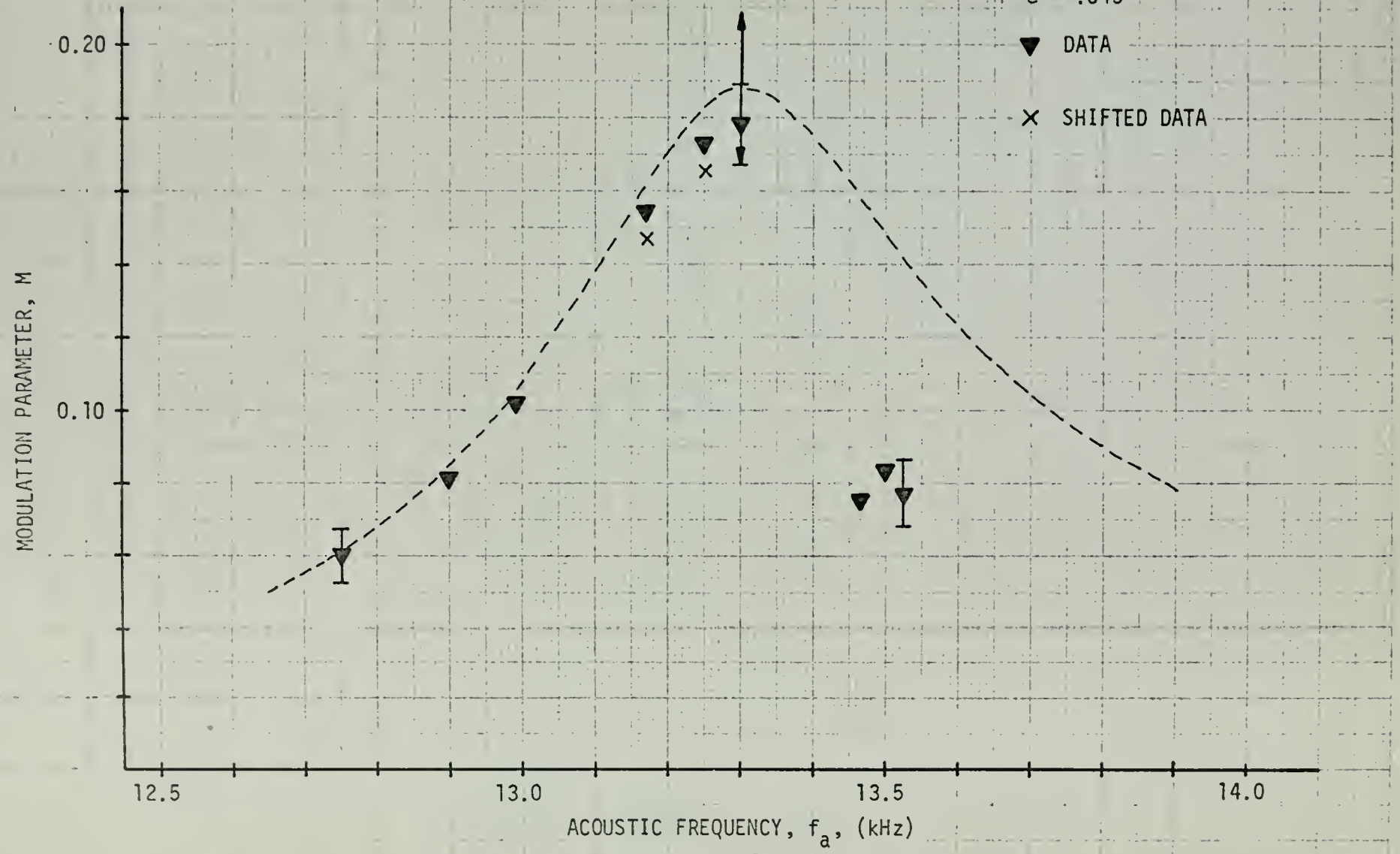
PROBE POSITION 42 cm
ε = .043
DATA
SHIFTED DATA
0.20
0.10
MODULATION PARAMETER, M
12.5
13.0
13.5
14.0
ACOUSTIC FREQUENCY, f_a, (kHz)

FIGURE 28

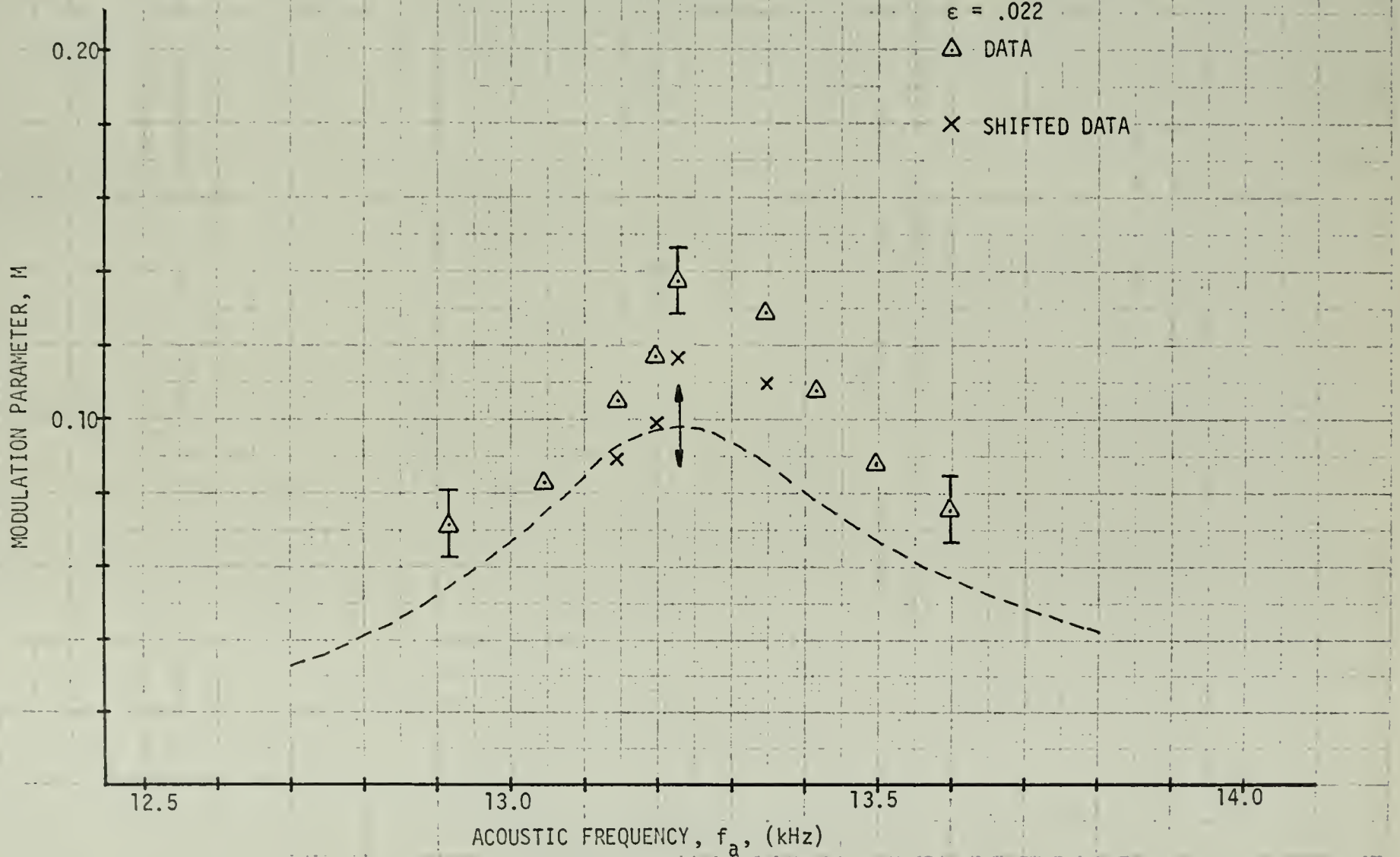
PROBE POSITION 67 cm
ε = .022
DATA
SHIFTED DATA
0.20
0.10
MODULATION PARAMETER, M
12.5
13.0
13.5
14.0
ACOUSTIC FREQUENCY, f_a, (kHz)

FIGURE 29

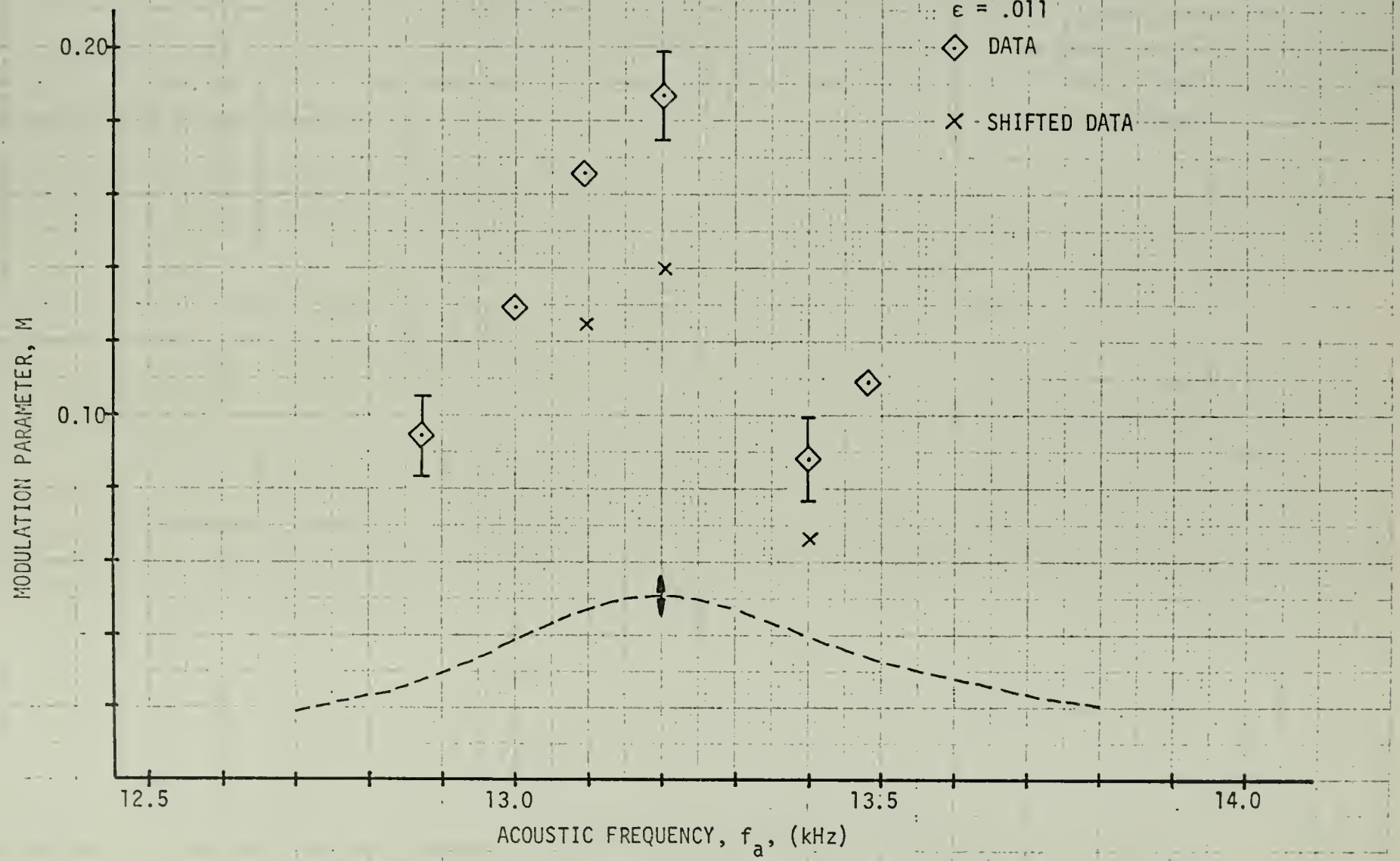
PROBE POSITION 90cm
ε = .011
DATA
SHIFTED DATA
0.20
0.10
MODULATION PARAMETER, M
12.5
13.0
13.5
14.0
ACOUSTIC FREQUENCY, f_a, (kHz)

FIGURE 30

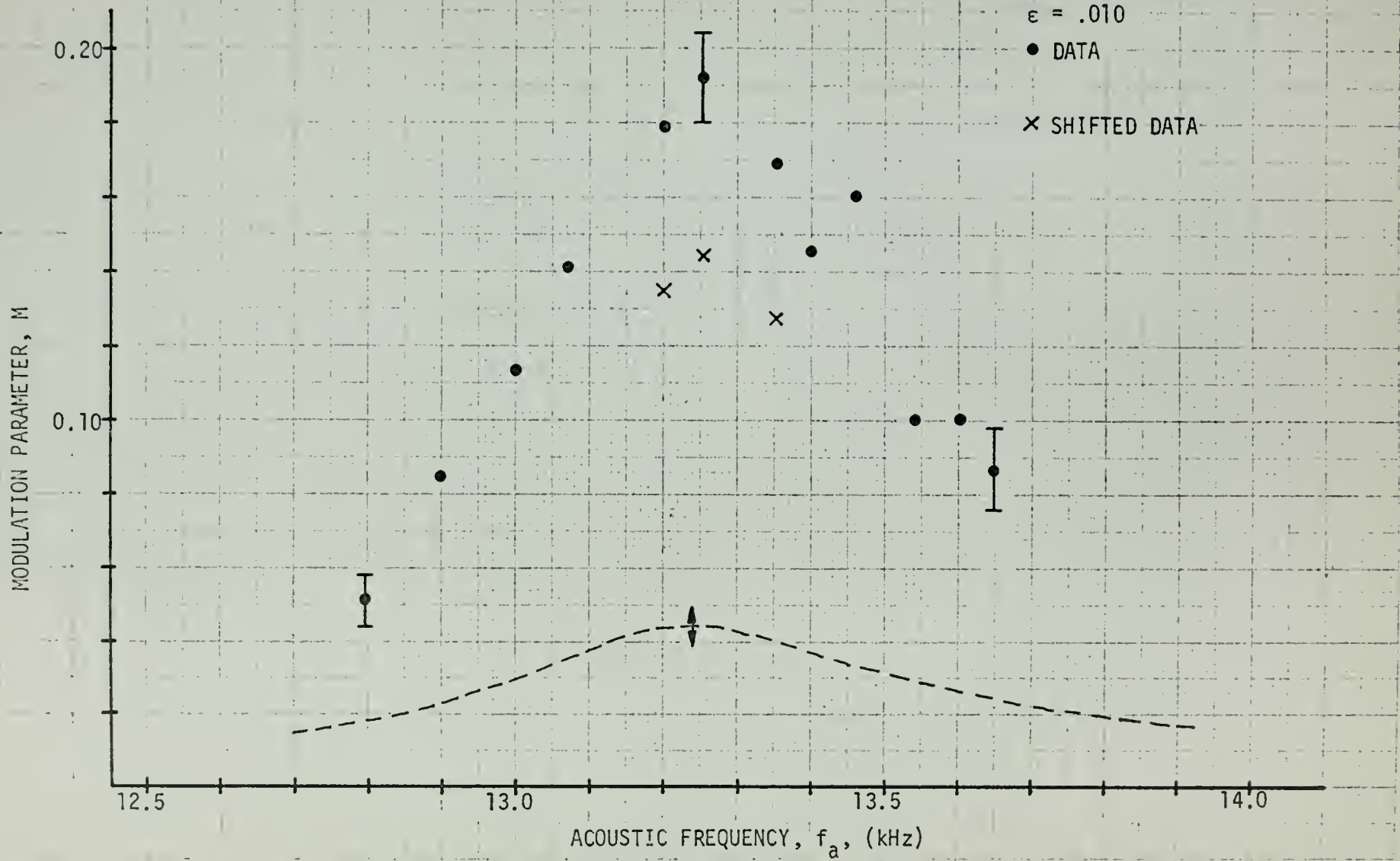
PROBE POSITION 90 cm
ε = .010
● DATA
× SHIFTED DATA
0.20
0.10
MODULATION PARAMETER, M
12.5
13.0
13.5
14.0
ACOUSTIC FREQUENCY, f_a, (kHz)

FIGURE 31

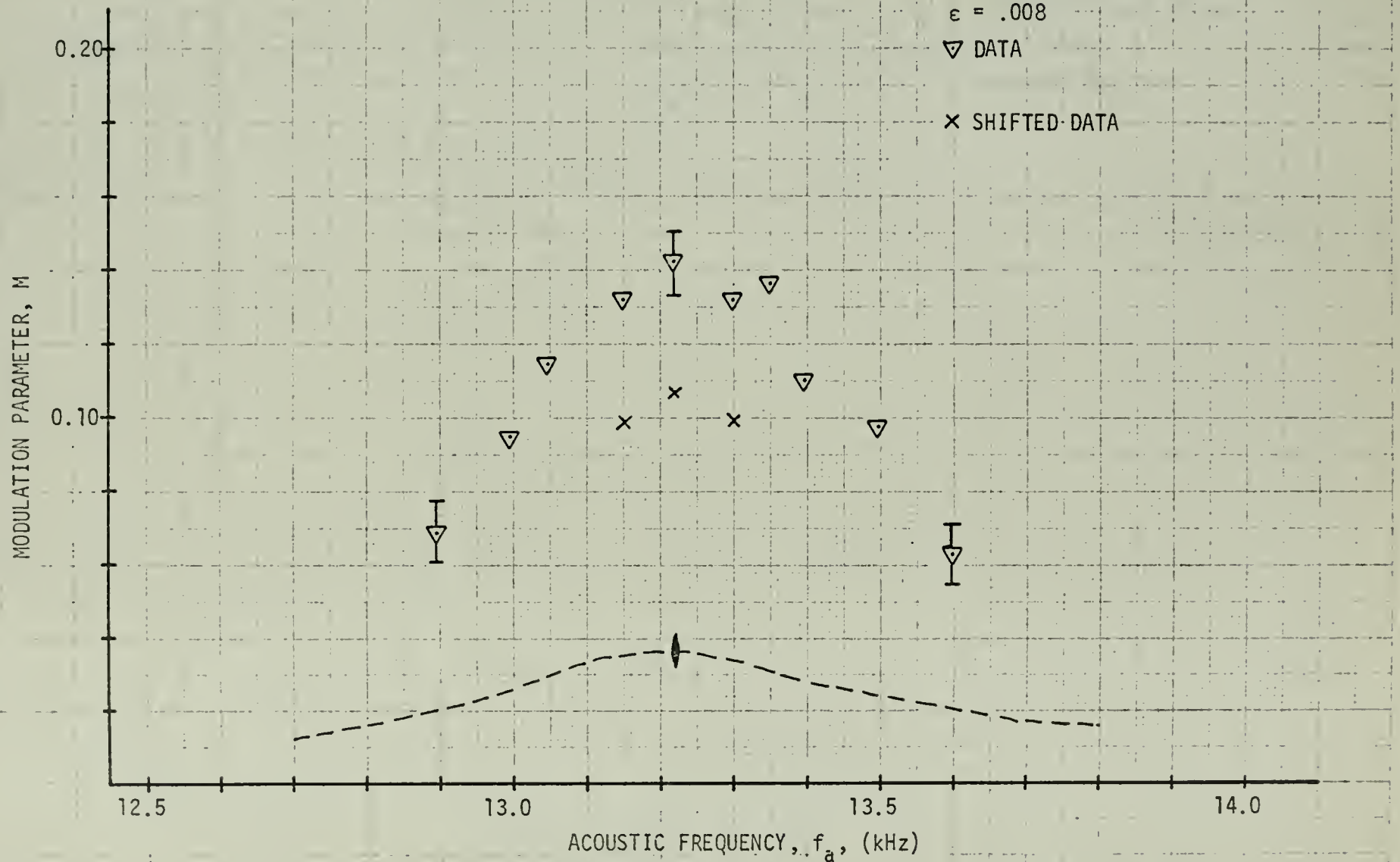
PROBE POSITION 100 cm
ε = .008
DATA
SHIFTED DATA
0.20
0.10
MODULATION PARAMETER, M
12.5
13.0
13.5
14.0
ACOUSTIC FREQUENCY, f_a, (kHz)

FIGURE 32

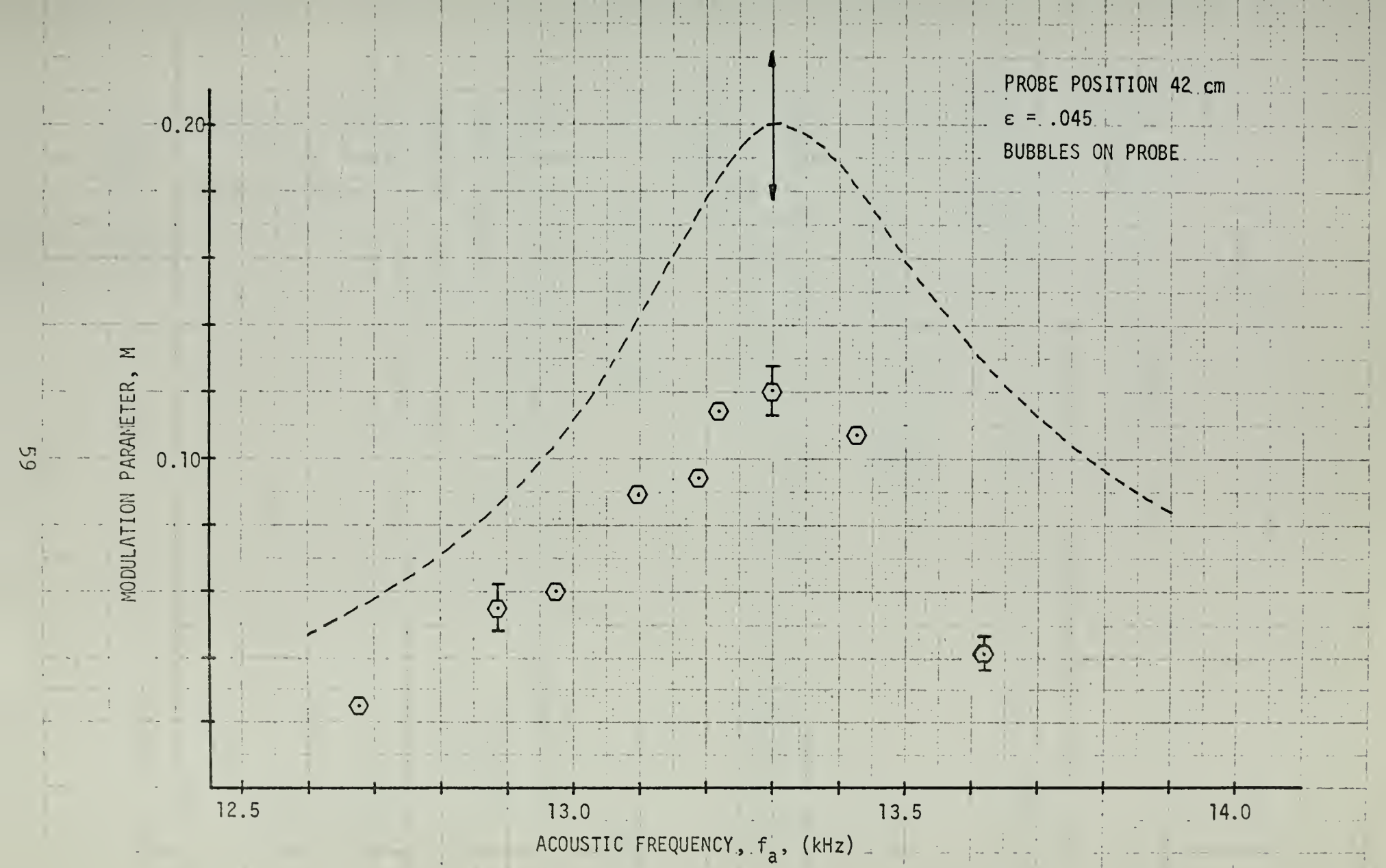
PROBE POSITION 42 cm
ε = .045
BUBBLES ON PROBE
0.20
0.10
MODULATION PARAMETER, M
12.5
13.0
13.5
14.0
ACOUSTIC FREQUENCY, f_a, (kHz)

FIGURE 33

$$\varepsilon = \varepsilon_o e^{-\delta x} \tag{3.6}$$

This resulted in a cumulative error in the in situ measurement of ±7 %.

The assumed 1 % deviation in the dimensions of the waveguide leads to a ±1.5 % error in the value of k_x. Examination of Eq. 2.13

$$K_z \doteq k_z \sqrt{1 - \frac{1 - 2k_x/\gamma}{(k_z/\gamma)^2}} \tag{3.7}$$

shows that an error of approximately ±3 % in K_z could result.

At resonance, the spatial decay in the z-direction can be written

$$\beta \doteq \frac{(2\eta + \delta)k_x}{K_z} \tag{3.8}$$

The value of the acoustic absorption coefficient in the x-direction, η, was of the order 2×10^{-3}. During the measurement of η it was not possible to discern nodes and antinodes since the standing wave ratio was very nearly one. Since the slope of the semi-log plot of acoustic amplitude vs distance was so slight it was possible to make a "worst case" error estimate of the value of η of ±100 %. However, the order of magnitude of the surface wave attenuation constant, δ, was 3×10^{-2}, large when compared to η. Thus, the combined error of the term $(2\eta + \delta)$ was approximately 8 %.

The equation for the modulation parameter, M, can be written

$$M = \left[\frac{1}{2}\varepsilon\pi\exp(-\gamma x)\right] \frac{\sin(\pi z/\ell_z)}{\left[(\Delta K_z \ell_z)^2 + (\beta\ell_z)^2\right]^{\frac{1}{2}}} \qquad (3.9)$$

The term $\sin(\pi z/\ell_z)$, when expanded, leads to an approximate error of 1 % from dimensional considerations. Thus, at resonance, the total error in M was approximately 11 %, considering all sources of error to be random. In Figures 26 - 33, this 11 % error is shown on the dashed plot of the theoretical modulation parameter as vertical arrows. The error flags plotted on representative data are indicative of a 12.5 % measurement error at low modulation, and a 6.5 % error at high modulation.

There was a variation in the modulation parameter at the resonant frequency which could be attributed to a standing surface wave. The theoretical predictions for a standing surface wave were not developed in this work. Unfortunately it had been decided to take all data at positions of the relative maximum modulation. These positions were seen to be separated by integer multiples of the half wavelength of the surface wave, consistent with the presence of a standing surface wave in addition to the traveling wave. The variation of the observed modulation parameter appeared to range from an estimated 10 % at the 42 cm position to as high as

50 % at the 90 and 100 cm positions. Representative data, corrected for this variable error are plotted as X's in Figures 26 - 32.

The variation in the maximum modulation parameter was the greatest source of error. While the error flags on the theoretical curves and data are indicative of the exactness of the waveguide and preciseness of the measurements taken, there was little basis upon which an estimation of how well the traveling wave condition had been achieved.

IV. RESULTS AND CONCLUSIONS

The experimental results consist primarily of two sets of data. The first set, shown in Figure 22, shows excellent correlation with theory and proves that there exists an infinite number of perturbation resonance conditions for the modulation of the acoustic signal. The fundamental perturbation resonance occurs when the surface wavelength is one-half the acoustic wavelength. The higher perturbation resonances occur for a linear relationship between the dimensionless parameters (k_x/γ) and $(k_z/\gamma)^2$. Although a complete set of integer values of m/n was not investigated due to frequency considerations, it can be implied from the data presented that perturbation resonances occur at all integer combinations of m/n.

The absorption coefficient of the surface wave increases linearly with frequency as shown in Figure 34. The data, taken over a period of several days, had a 96 % correlation to the straight line plotted with the data. At frequencies lower than those shown on the graph, a sizable standing surface wave developed, making it difficult to observe the absorption coefficient. Due to the relatively short path length for the acoustic wave, the relationship between the acoustic signal in the x-direction and the acoustic frequency was not determined.

There exist many degenerate perturbation modes where the acoustic resonant frequency and the surface wave number,

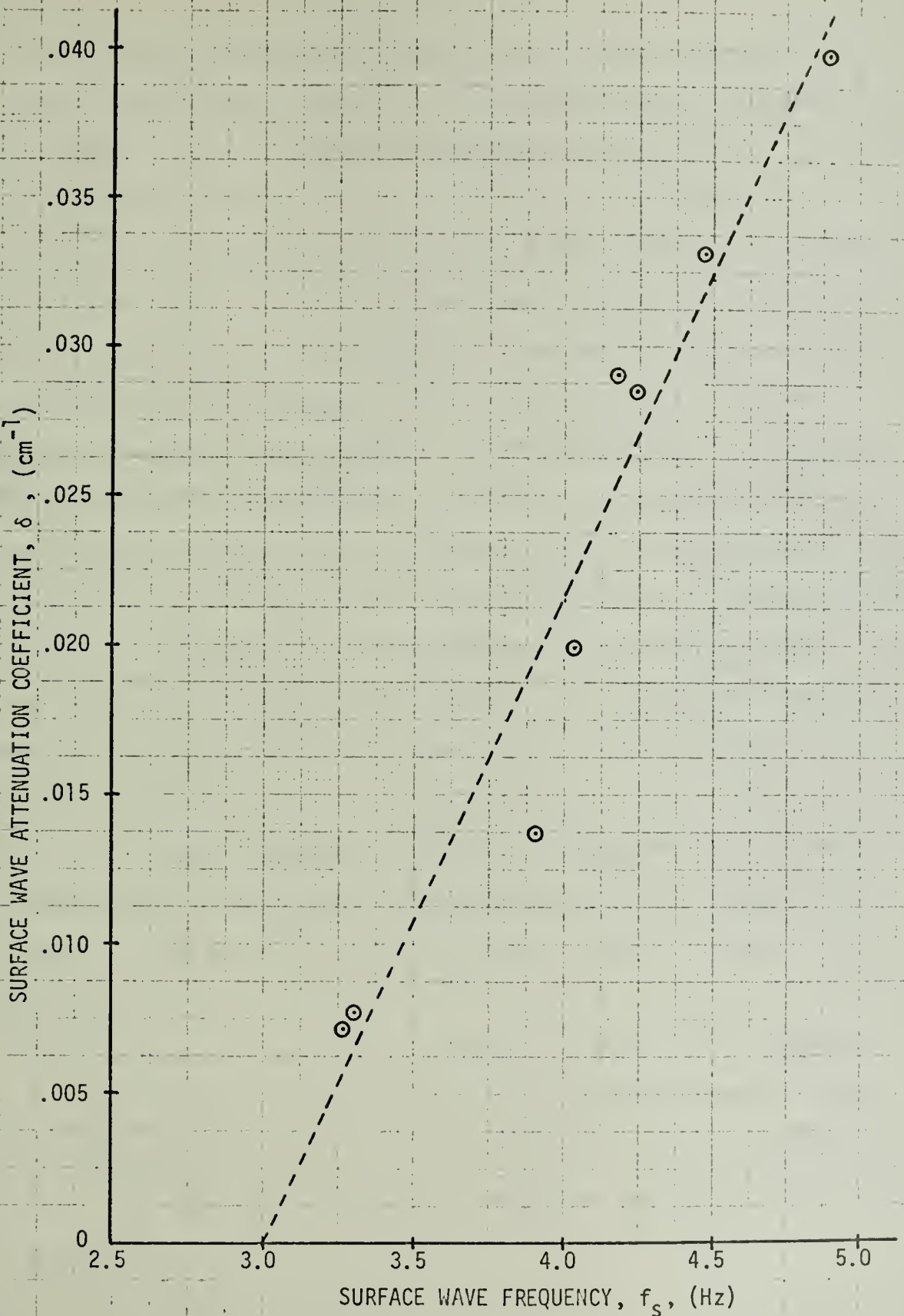
.040
.035
.030
.025
.020
.015
.010
.005
0
SURFACE WAVE ATTENUATION COEFFICIENT, δ , (cm⁻¹)
2.5
3.0
3.5
4.0
4.5
5.0
SURFACE WAVE FREQUENCY, f_s, (Hz)

FIGURE 34

γ, are coincident for different normal modes. These degeneracies are listed in Table 1. In addition to these modes, there are several singular degeneracies where curves cross at only one point.

There is excellent correlation between the data presented in Figures 26 - 29 and the predicted behavior of the modulation parameter in the vicinity of resonance. There is consistency in the bandwidth of all the other data sets and the theoretical bandwidths; but, as can be seen in Figures 30 -32 there is considerable deviation in the amplitude of the predicted and measured modulation at the 90 cm and 100 cm positions. Two factors may have contributed to this variation:

1. Beyond the 90 cm position, it was noted that the surface wave attenuation constant was no longer linear, indicating an apparent decrease in the rate of decay of the surface wave.

2. The standing wave noted previously at the low surface wave frequencies was probably present, though undetected at the higher frequency used in this section of the experiment.

It would be expected that standing wave effects would not more than double the modulation parameter even at their worst, whereas a factor of approximately four was experienced. This is an area which should be examined more fully in future experiments.

The deviation of data below the predicted modulation parameter seen in Figure 33 was due to the presence of bubbles on the acoustic probe. The pressure-release boundary created on the surface of the probe by the bubbles had the expected effect of decreasing the sensitivity of the probe and a decrease in signal amplitude resulted.

There are several considerations which should be made before next attempting this experiment:

1. Extreme care should be taken to ensure that the waveguide dimensions are exact. This could be accomplished by constructing the support walls of metal, which should be machined if necessary to produce absolutely uniform dimensions. In addition, the pressure release walls should be made from styrofoam, planed to desired dimensions, instead of polyurethane which is not as sturdy.

2. More careful attention should be given to the construction of a termination which would more adequately absorb surface wave energy. The exponential horn could be lengthened and the surface wave could be channeled to many small absorption chambers by means of thin, sound-absorbent dividers. It is believed that this modification would not adversely effect the excellent acoustic termination achieved in this experiment.

3. A design for automated data taking should be conceived. This would require a detector to separate the modulation from the acoustic signal, and a means for automatically

recording the modulation as the probe is traversed down the waveguide.

BIBLIOGRAPHY

1. J. W. Strutt Lord Rayleigh, The Theory of Sound, p. 89-96, Dover Publications, Inc., 1945.

2. Samuels, J. C., "On Propagation of Waves in Slightly Rough Ducts," J. Acoust. Soc. Am., v. 31, p. 319-325, March 1959.

3. Salant, R. F., "Acoustic-Wave Propagation Past a Sinusoidal Surface," J. Acoust. Soc. Am., v. 44, p. 38-40, July 1968.

4. Salant, R. F., "Acoustic Propagation in Waveguides with Sinusoidal Walls," J. Acoust. Soc. Am., v. 53, p. 504-507, February 1973.

5. Nayfeh, A. H., "Sound Waves in Two-dimensional Ducts with Sinusoidal Walls," J. Acoust. Soc. Am., v. 56, p. 768-770, September 1974.

6. Jordan, Jr., W. E., Preliminary Investigation of the Effect of Surface Fluctuations on Sound Amplitude in Guided Mode Propagation, Master's Thesis, Naval Postgraduate School, Monterey, California, 1970.

7. Ebert, R. H., A Study of the Influence of Gravity Waves in a Water Filled Waveguide, Master's Thesis, Naval Postgraduate School, Monterey, California, 1971.

8. Coppens, A. B., Private Communication.

9. Kinsman, B., Wind Waves, p. 126-133, Prentice-Hall, Inc., 1965.

INITIAL DISTRIBUTION LIST

		No. Copies
1.	Defense Documentation Center Cameron Station Alexandria, Virginia 22314	2
2.	Library, Code 0212 Naval Postgraduate School Monterey, California 93940	2
3.	Department Chairman, Code 61 Department of Physics and Chemistry Naval Postgraduate School Monterey, California 93940	2
4.	Assoc. Professor A. B. Coppens, Code 61Cz Department of Physics and Chemistry Naval Postgraduate School Monterey, California 93940	2
5.	Department Library, Code 61 Department of Physics and Chemistry Naval Postgraduate School Monterey, California 93940	1
6.	LCDR Norman E. Davis, USN 1227 Leahy Road Monterey, California 93940	1
7.	LCDR Morton W. Kenyon, USN 316 Crystal Avenue New London, Connecticut 06320	1
8.	Dr. David T. Blackstock Applied Research Laboratories University of Texas Austin, Texas 78712	1

Thesis
D1725 Davis
c.1
156667
A preliminary study of a surface wave-acoustical normal mode resonance in a fluid-filled rectangular waveguide with pressure-release boundaries.